Stereospecific Formation of Interstrand Carbinolamine DNA Cross-Links by Crotonaldehyde- and Acetaldehyde-Derived α-CH 3 -γ-OH-1, N 2 -Propano-2‘-deoxyguanosine Adducts in the 5‘-C...

ARTICLE *in* CHEMICAL RESEARCH IN TOXICOLOGY · MARCH 2006

Impact Factor: 3.53 · DOI: 10.1021/tx050239z · Source: PubMed

11 AUTHORS, INCLUDING:

Markus Voehler
Vanderbilt University
49 PUBLICATIONS **876** CITATIONS
SEE PROFILE

Jarrod Anson Smith
Vanderbilt University
27 PUBLICATIONS **732** CITATIONS
SEE PROFILE

Thomas Harris
Vanderbilt University
330 PUBLICATIONS **8,672** CITATIONS
SEE PROFILE

R. Stephen Lloyd
Oregon Health and Science University
224 PUBLICATIONS **6,850** CITATIONS
SEE PROFILE

Published in final edited form as:
Chem Res Toxicol. 2006 February ; 19(2): 195–208. doi:10.1021/tx050239z.

Stereospecific Formation of Interstrand Carbinolamine DNA Crosslinks by Crotonaldehyde- and Acetaldehyde-Derived α-CH_3-γ-OH-1,N^2-Propano-2'-deoxyguanosine Adducts in the 5′-CpG-3′ Sequence

Young-Jin Cho, **Hao Wang**, **Ivan D. Kozekov**, **Andrew J. Kurtz**[*], **Jaison Jacob**[§], **Markus Voehler**, **Jarrod Smith**, **Thomas M. Harris**, **R. Stephen Lloyd**[‡], **Carmelo J. Rizzo**, and **Michael P. Stone**[†]

Department of Chemistry, Center in Molecular Toxicology, Vanderbilt-Ingram Cancer Center, Vanderbilt University, Nashville, Tennessee 37235

Abstract

The crotonaldehyde- and acetaldehyde-derived *R*- and *S*-α-CH_3-γ-OH-1,N^2-propanodeoxyguanosine adducts were monitored in single-stranded and duplex oligodeoxynucleotides using NMR spectroscopy. In both instances the *cis* and *trans* diastereomers of the α-CH_3 and γ-OH groups underwent slow exchange, with the *trans* diastereomers being favored. In single-stranded oligodeoxynucleotides, the aldehyde intermediates were not detected spectroscopically, but their presence was revealed through the formation of N-terminal conjugates with the tetrapeptide KWKK. When annealed into 5′-d(GCTAGCXAGTCC)-3′•5′-d(GGACTCYCTAGC)-3′ containing the 5′-CpG-3′ sequence context (X=*R*- or *S*-α-CH_3-γ-^{13}C-OH-PdG; Y=$^{15}N^2$-dG), at pH 7, partial opening of the *R*- or *S*-α-CH_3-γ-^{13}C-OH-PdG adducts to the corresponding N^2-(3-oxo-1-methyl-propyl)-dG aldehydes was observed at temperatures below the T_m of the duplexes. These aldehydes equilibrated with their geminal diol hydrates; higher temperatures favored the aldehydes. When annealed opposite to T, the *S*-α-CH_3-γ-^{13}C-OH-PdG adduct was stable. At 37 °C, an interstrand DNA crosslink was observed spectroscopically only for the *R*-α-CH_3-γ-OH-PdG adduct. Molecular modeling predicted that the interstrand crosslink formed by the *R*-α-CH_3-γ-OH-PdG adduct introduced less disruption into the duplex structure than did the crosslink arising from the *S*-α-CH_3-γ-OH-PdG adduct, due to differing orientations of the *R*- and *S*-CH_3 groups. Modeling also predicted that the α-methyl group of the aldehyde arising from the *R*-α-CH_3-γ-OH-PdG adduct oriented in the 3′ direction in the minor groove, facilitating crosslinking. In contrast, the α-methyl group of the aldehyde arising from the *S*-α-CH_3-γ-OH-PdG adduct oriented in the 5′ direction within the minor groove potentially hindering crosslinking. NMR revealed that for the *R*-α-CH_3-γ-OH-PdG adduct, the carbinolamine form of the crosslink was favored in duplex DNA, *in situ*, with the imine or Schiff base form of the crosslink remaining below the level of spectroscopic detection. Molecular modeling predicted that the carbinolamine linkage maintained Watson-Crick hydrogen bonding at both of the tandem C•G base pairs. Dehydration of the carbinolamine crosslink to an imine, or cyclization of the latter to form a pyrimidopurinone crosslink, required disruption of Watson-Crick hydrogen bonding at one or both of the crosslinked base pairs.

†Author to whom correspondence should be addressed. Telephone 615-322-2589; FAX 615-322-7591; email michael.p.stone@vanderbilt.edu.
[§]Current Address for Jaison Jacob: Wyeth Pharmaceuticals, 35 Cambridge Park Drive, Cambridge, MA 02140
[‡]Center for Research on Occupational and Environmental Toxicology, Oregon Health and Science University, 3181 SW Sam Jackson Park Road, L606, Portland, OR 97239-3098
[*]Current Address for Andrew J. Kurtz: Department of Human Biological Chemistry and Genetics, University of Texas Medical Branch, Galveston, Texas 77555-1068

Introduction

Crotonaldehyde **1**, an α,β-unsaturated aldehyde, is genotoxic and mutagenic in human lymphoblasts (1). It induces liver tumors in rodents (2). Michael addition of crotonaldehyde to deoxyguanosine yields the enantiomeric *R*- and *S*-α-CH_3-γ-OH-1,N^2-propano-2'-deoxyguanosine adducts **2a** and **2b** (Scheme 1) (3–6); a second DNA adduction pathway yields paraldol-releasing DNA adducts (7), primarily N^2-(3-hydroxybutylidene)-dG (8). Adducts **2a** and **2b** and are also formed through the reaction of acetaldehyde, a mutagen and potential human carcinogen (9), with deoxyguanosine (6,10). The *R*- and *S*-α-CH_3-γ-OH-PdG adducts **2a** and **2b** were detected in human and rodent tissues (11,12). In humans, these probably result from various endogenous and exogenous exposures, including lipid peroxidation (11,13,14), exposure to tobacco smoke (15,16), and exposure to N-nitrosopyrrolidine (17,18).

Adducts **2a** and **2b** are structurally analogous to the major adduct produced by the reaction of acrolein with DNA, γ-OH-PdG (11,13,14,19,20). When placed opposite dC, opening of the γ-OH-PdG adduct resulted in formation of the N^2-(3-oxopropyl)-dG aldehyde, and its hydrate, which oriented into the minor groove of the DNA (21). The presence of the N^2-(3-oxopropyl)-dG aldehyde in the minor groove facilitated DNA interstrand crosslinking. In the 5′-CpG-3′ sequence context γ-OH-PdG formed crosslinks that were isolated, following $NaCNBH_3$ reduction, as saturated three-carbon interstrand N^2,N^2-dG linkages (22,23). NMR analysis of the crosslinks, in duplex DNA, *in situ*, identified them as carbinolamines (24,25). The γ-OH-PdG adduct also formed crosslinks with the N-terminal amine of the peptide KWKK (26).

The site-specific synthesis of oligodeoxynucleotides containing cyclic adducts **2a** or **2b** (22, 27,28) enabled their chemistry and biology to be examined in duplex DNA. In duplex DNA at neutral pH, adducts **2a** or **2b** exhibited chemistry similar to that of the γ-OH-PdG adduct. When adducts **2a** or **2b** were placed into oligodeoxynucleotide duplexes at 5′-CpG-3′ sequences, Kozekov et al. (23) trapped interstrand saturated three carbon crosslinks by treatment with $NaCNBH_3$, corroborating the reports of Wang et al. (6,8). Significantly, crosslinking was dependent upon the stereochemistry of the adduct, favoring the *R*-α-CH_3-γ-OH-PdG adduct **2a**, as opposed to the *S*-α-CH_3-γ-OH-PdG adduct **2b**. However, both the *R*-α-CH_3-γ-OH-PdG adduct **2a**, and the *S*-α-CH_3-γ-OH-PdG adduct **2b** readily formed N-terminal conjugates with the peptide KWKK (26). This implied that both the adducts **2a** and **2b** underwent opening to the corresponding aldehydes **3a** or **3b** when placed opposite dC in duplex DNA, but only aldehyde **3a** efficiently formed interstrand DNA crosslinks in the 5′-CpG-3′ sequence.

Nevertheless, the chemistry of adducts **2a** and **2b** in DNA, including the identity of the interstrand crosslink formed in the 5′-CpG-3′ sequence by adduct **2a**, remained elusive. The ability to trap a saturated three-carbon interstrand crosslink by treatment of the duplex with $NaCNBH_3$ implied the intermediacy of crosslinked imine **6a** (23). However, imine **6a** was anticipated to exist in equilibrium with carbinolamine **5a** and, potentially, pyrimidopurinone **7a** (23). Consistent with this expectation, ESI-Q-TOF mass spectrometry yielded signals consistent with the presence of carbinolamine **5a**, and imine **6a** and/or pyrimidopurinone **7a**, with the latter signal predominating (10). On this basis, Lao and Hecht suggested that the imine **6a** was the predominant species in duplex DNA, existing in equilibrium with the carbinolamine **5a** and the pyrimidopurinone **7a**. Consequently, it was of interest to examine the structures of crotonaldehyde- and acetaldehyde-derived adducts **2a** and **2b** in duplex DNA spectroscopically, and those of interstrand crosslinks in the 5′-CpG-3′ sequence.

In the present work, site-specific introduction of ^{13}C at the aldehydic C_γ of crotonaldehyde (Scheme 2 and Scheme 3) and of ^{15}N at the exocyclic amine of the targeted dG in the complementary strand of 5′-d(GCTAGC<u>X</u>AGTCC)-3′•5′-d(GGACTG<u>Y</u>CTAGC)-3′ (X=*R*- or

S- α-CH_3-γ-^{13}C-OH-PdG; Y=$^{15}N^2$-dG) (Scheme 4), enabled the chemistry of α-CH_3-γ-^{13}C-OH-PdG adducts **2a** and **2b** to be monitored. The chemistry of adducts **2a** and **2b** in duplex DNA, while similar to that of the acrolein-derived γ-OH-PdG adduct, differed in that the propensity for these 1,N^2-dG adducts to open to the corresponding N^2-(3-oxo-1-methyl-propyl)-dG aldehydes in duplex DNA was reduced. Moreover, their ability to form interstrand crosslinks in the 5′-CpG-3′ sequence was dependent upon stereochemistry of the methyl group at the α-carbon. Similar to the interstrand crosslink induced by the acrolein-derived γ-OH-PdG in the 5′-CpG-3′ sequence, crotonaldehyde-derived adduct **2a** yielded carbinolamine crosslink **5a**, with the corresponding imine **6a** remaining below the level of detection. Molecular modeling suggested that interstrand crosslinks arising from the *R*-α-CH_3-γ-OH-PdG adduct introduced less disruption into the duplex than did those arising from the *S*-α-CH_3-γ-OH-PdG adduct, due to differing orientations of the *R*- and *S*-CH_3 groups. Moreover, for the *R*-α-CH_3-γ-OH-PdG adduct **2a**, the methyl group was predicted to orient in the 3′ direction in the minor groove, favoring formation of carbinolamine crosslink **5a**. In contrast, the lower level of interstrand crosslinking observed for the *S*-α-CH_3-γ-OH-PdG adduct **2b** in the 5′-CpG-3′ sequence might be attributed, in part, to the unfavorable orientation of the methyl group in the 5′ direction within the minor groove, hindering reaction between aldehyde **3b** and the targeted dG in the complementary strand. Modeling studies also predicted that the carbinolamine crosslink observed for the *R*-α-CH_3-γ-OH-PdG adduct maintained Watson-Crick hydrogen bonding at both of the tandem C•G base pairs. Dehydration of the carbinolamine crosslink to an imine, or cyclization of the latter to form a pyrimidopurinone crosslink, required disruption of Watson-Crick hydrogen bonding at one or both of the crosslinked base pairs.

Materials and Methods

Oligodeoxynucleotide synthesis

The preparation of non-isotopically labeled oligodeoxynucleotides containing site-specific γ-OH-PdG and α-CH_3-γ-OH-PdG adducts has been described (22,27,28). All commercially obtained chemicals were used as received. Methylene chloride was freshly distilled from calcium hydride. Anhydrous THF was freshly distilled from a sodium/benzophenone ketyl. All reactions were performed under argon atmosphere. Glassware was oven dried and cooled under argon. Concentrations of the single-stranded oligodeoxynucleotides were determined from calculated extinction coefficients at 260 nm (29). The purities of the modified oligodeoxynucleotides were analyzed using a PACE 5500 capillary electrophoresis (Beckman Instruments, Inc., Fullerton, CA) instrument. Electrophoresis was conducted using an eCAP ssDNA 100-R kit applying 12,000 V for 30 min. The electropherogram was monitored at 254 nm. MALDI-TOF mass spectra were measured on a Voyager-DE (PerSeptive Biosystems, Inc., Foster City, CA) instrument in negative reflector mode. The matrix contained 0.5 M 3-hydroxypicolinic acid and 0.1 M ammonium citrate.

Stereospecific synthesis of aminodiols 4-(*R*)- and 4(*S*)-aminopentane-1,2-^{13}C-diol (14a, 14b)

These were prepared using identical methods starting with (*R*)- or (*S*)-2-amino-1-propanols respectively; the synthesis of 4(*S*)-aminopentane-1,2-(^{13}C)-diol **14b** is provided below.

tert-Butoxy (2-hydroxy-1(*S*)-methylethyl)carbamate (9b)

To a stirred solution of (*S*)-2-amino-1-propanol (**8b**, 0.38 g, 5 mmol) and 1N NaOH (5 mL) cooled to 0° C, was added dropwise di-*tert*-butyl dicarbonate (1.2 g, 5.5 mmol) in CH_2Cl_2 (10 mL). The mixture was stirred at room temperature overnight. The layers were separated and the organic phase was sequentially washed with 0.1 N HCl, 5% $NaHCO_3$ and brine, and dried over $MgSO_4$ and concentrated. Purification by flash chromatography on silica, eluting with 2–3% CH_3OH in $CHCl_3$, gave **9b**, (0.714 g, 81.5 %): ^{1}H NMR ($CDCl_3$) δ 4.72 (br, 1H), 3.76 (m, 1H), 3.63 (m, 1H), 3.50 (m, 1H), 1.44 (s, 9H), 1.14 (m, 3H).

tert-Butoxy (2-(¹³C-cyano)-1(*S*)-methylethyl)carbamate (10b)

To a stirred solution of **9b** (395 mg, 2.25 mmol) and trimethylamine (0.50 mL, 9.41 mmol, 3.6 mmol) in anhydrous CH_2Cl_2 (5 mL) cooled to 0° C, was added dropwise a solution of methanesulfonyl chloride (310 mg, 2.64 mmol) in anhydrous CH_2Cl_2 (2 mL). The reaction was stirred at room temperature for 2 h. The solution was then washed with saturated $NaHCO_3$ solution. The organic layer was separated, dried over K_2CO_3 and concentrated *in vacuo*. The crude mesylate was dissolved in DMSO (10 mL) and $K^{13}CN$ (237 mg, 3.6 mmol), which had been dried in the oven and ground into a powder, was added. The reaction was stirred at 40° C for 15 hr. After cooling at room temperature, water (20 mL) was added and the mixture was extracted with ether (3 × 10 mL). The combined organic phases were washed with a saturated brine (3 × 10 mL), dried over $MgSO_4$, filtered, and concentrated *in vacuo*. Flash chromatography eluting with 12–15% ethyl acetate in hexane gave **10b** (286 mg, 69.0%): ^{1}H NMR ($CDCl_3$) δ 4.62 (br, 1H), 3.96 (m, 1H), 2.80 (m, 1H), 2.56 (m, 1H), 1.45 (s, 9H), 1.32 (d, 3H, J = 6.8 Hz).

tert-Butoxy (1(*S*)-methyl-3-¹³C-oxopropyl)carbamate (11b)

A solution of **10b** (258 mg, 1.4 mmol) in anhydrous CH_2Cl_2 (3 mL) was cooled to −78° C, then DIBAL-H (1.0 M in CH_2Cl_2 , 2.1 mL) was added dropwise over 20 min. The reaction was stirred below −70° C for 10 min, then quenched by the addition of acetone (1 mL) followed by saturated NH_4Cl (10 mL). The resulting mixture was allowed to warm to room temperature and stirred for 40 min. The mixture was filtered through a pad of Celite and the filtrate was washed with brine, dried over $MgSO_4$ and concentrated *in vacuo*. Purification by flash chromatography on silica gel, eluting with 20–25% ethyl acetate in hexane, gave **11b** (88 mg, 32 %)[2]: ^{1}H NMR ($CDCl_3$) δ 10.05 and 9.47 (d × m, 1H, $J_{C\text{-}H}$= 175.5 Hz), 4.99 (br, 1H), 4.14 (m, 1H), 2.64 (m, 2H), 1.43 (s, 9H), 1.23 (m, 3H).

tert-Butoxy (1(*S*)-methylprop-3-¹³C-enyl)carbamate (12b)

To a stirred suspension of methyltriphenylphosphonium bromide (214 mg, 0.6 mmol) in THF (5 mL) was added a solution of potassium *tert*-butoxide (1M in THF; 56 μL, 0.56 mmol)] and the resulting solution stirred for 30 min. The solution was cooled to 0 °C, then a solution of **11b** (88 mg, 0.47 mmol) in THF (2 mL) was added dropwise. After the addition was complete, the reaction was warmed to room temperature and stirred for 1 h. The reaction was then quenched by the addition of saturated aqueous NH_4Cl and the layers separated. The aqueous phase was extracted with ether (3×20 mL), dried over Na_2SO_4, and concentrated *in vacuo*. Purification by flash chromatography on silica gel, eluting with 3% ethyl acetate in hexane, gave **12b** (61 mg, 70.0%) as a colorless oil: $[\alpha]^{20}_D$ –19.3° (*c* 1.10, $CHCl_3$); ^{1}H NMR ($CDCl_3$) δ 5.96 and 5.58 (d×m, 1H, $J_{C\text{-}H}$ = 144 Hz), 5.01 (m, 2H), 4.38 (br, 1H), 3.73 (m, 1H), 2.20 (m, 2H), 1.44 (s, 9H), 1.12 (d, 3H, *J* = 6.6 Hz).

tert-Butoxy (1(*S*)-methyl-[3,4-dihydroxy-3-¹³C-propyl]) (13b)

To a stirred solution of **12b** (42 mg, 0.225 mmol), *N*-methylmorpholine *N*-oxide (30 mg, 0.248 mmol), THF (0.8 mL), *t*- BuOH (0.32 mL), and water (0.16 mL) was added osmium tetroxide (10 μL, 0.1 M solution in benzene, 1.0 μmol). The mixture was stirred for 12 h and then a second portion of osmium tetroxide (6 μL, 0.1 M solution in benzene, 0.6 μmol) was added and stirring continued for an additional 8 h. The reaction was then quenched with 5% aqueous $NaHSO_3$ (5 mL) with vigorously stirring for 15 min then poured into water (10 mL) and extracted with methylene chloride (3 _ 10 mL). The combined organic extracts were dried over Na_2SO_4, filtered and concentrated *in vacuo*. Purification by flash chromatography on silica, eluting with 1–2 % methanol in chloroform, gave **13b** (37.5 mg, 76.0 %) as an inseparable mixture of diastereomers: ^{1}H NMR (major, $CDCl_3$) δ 4.55-4.50 (m, 2H, NH, OH), 3.95 (m, 1H), 3.93 and 3.47 (d×m, 1H, $J_{C\text{-}H}$ = 138 Hz), 3.50 (m, 2H), 2.48 (br, 1H, OH), 1.53 (m, 1H),

1.45 (s, 9H), 1.26 (m, 1H), 1.19 (d, 3H, *J* = 6.7 Hz); (minor, $CDCl_3$) δ 4.61 (m, 1H), 4.04 & 3.57 (m and m, 1H, *J* = 142 Hz), 3.79 (m, 1H), 3.64 (m, 1H), 3.47 (m, 1H), 3.22 (br, 1H), 2.40 (br, 1H), 1.60 (m, 2H), 1.44 (s, 9H), 1.19 (d, 3H, J = 6.6 Hz).

4(*S*)-amino-1,2-dihydroxy-2-^{13}C-pentane (14b)

To a solution of **13b** (30 mg, 0.136 mmol) in CH_2Cl_2 (1.5 mL) and methanol (0.5 mL) was added H-Amberlyst 15 resin (0.3 g). The mixture was gently shaken over 14 h until TLC analysis showed the complete disappearance of **13b**. The resin was removed by filtration and successively washed with THF and methanol. This amine-bound resin was transferred to a solution of 4 M ammonia in methanol and gently shaken for 50 min. The resin was then removed by filtration and washed with methanol (3 × 5 mL). The combined filtrates were evaporated *in vacuo* to give **14b** (15 mg, 91%) which was used without further purification: ^{1}H NMR (CD_3OD) δ 3.94 & 3.58 (m and m, 1H, *J* = 144 Hz), 3.45 (m, 2H), 3.24 (m, 1H), 1.56 (m, 2H), 1.18 (d, 3H, *J* = 6.5 Hz).

Synthesis of stereoisomeric *R*-and *S*-α-CH_3-γ-^{13}C-OH-PdG oligodeoxynucleotides

The O^6-TMSE-2-fluoroinosine-modified oligodeoxynucleotide **15** (125 A_{260} units) (30,31) was mixed in a plastic test tube with diisopropylethylamine (150 μL), DMSO (300 μL), and either 4(*R*)- or 4(S)-aminopentane-1,2-(^{13}C)-diol (**14a**, **14b**) (5 mg). The reaction mixtures were stirred at 55 °C for 24 h. The solvents were evaporated *in vacuo* using a centrifugal evaporator. The residues were dissolved in 5% acetic acid (500 μL) and stirred for 2 h at room temperature to remove the O^6-TMSE group. The mixtures were neutralized with 1 M NaOH and purified by HPLC using gradient A (see below) to give the corresponding stereoisomeric N^2-(1-methyl-3,4-dihydroxybutyl)guanine-modified oligodeoxynucleotides **16a and b**. ^{13}C-labeled *R*-stereoisomer: 54.0 A_{260} units (43%). MALDI-TOF MS: calcd for $[M - H]^-$ 3747.7, found 3747.4. ^{13}C-labeled *S*-stereoisomer: 65.0 A_{260} units (52%); MALDI-TOF MS: calcd for $[M - H]^-$ 3747.7, found 3747.1

An aqueous solution of $NaIO_4$ (500 μL, 20 mM) was added to solutions of N^2-(1-methyl-3,4-dihydroxybutyl)guanine-modified oligodeoxynucleotides **16**, **16b** (54.0 A_{260} units) in 0.05 M, pH 7.0 phosphate buffer, (500 μL) and the reaction mixtures were stirred at room temperature for 10 min. The mixtures were purified by HPLC using gradient B (see below) to give 8-hydroxy-6(*S or R*)-methyl-5,6,7,8-tetrahydropyrimido[1,2-*a*]purin-10(3*H*)-one) adducts **17a and b**. ^{13}C-labeled *R*-stereoisomer: 41.8 A_{260} units (77%); MALDI-TOF MS: calcd for $[M - H]^-$ 3715.7, found 3715.7. ^{13}C-labeled *S*-stereoisomer: 61.5 A_{260} units (90%) from 65 A_{260} units MALDI-TOF MS: calcd for $[M - H]^-$ 3715.7, found 3716.6.

Synthesis of $^{15}N^2$-dG-modified complementary oligodeoxynucleotide 5′-GGACTCGCTAGC-3′

The O^6-TMSE-2-fluoroinosine-modified oligodeoxynucleotide (31) was deprotected using 6 M $^{15}NH_4OH$, desilyated with 5 % acetic acid, and purified by C8 HPLC in 0.1 M ammonium formate (pH 6.5), yielding the $^{15}N^2$-dG-modified oligodeoxynucleotide. Negative ion MALDI-TOF mass spectrometry yielded m/z 3645.9 (calcd for $[M-H]^-$ 3645.6).

HPLC separations

The purifications of oligodeoxynucleotides **16a**, **16b** and **17a**, **17b** were performed on a Beckman HPLC system (32 Karat software version 3.1, pump module 125) with a diode array UV detector (module 168) monitoring at 260 nm using Phenomenex Luna 5μ C8 column (250 mm × 10 mm i.d., 3 mL/min for purification) with 0.1 M aqueous ammonium formate and CH_3CN for oligonucleotides. *HPLC gradients*: **A**) 1–7 % acetonitrile over 25 min, hold for 3 min, 7–99% acetonitrile over 2 min, hold for 5 min, hold for 2 min, and then to 1% acetonitrile

over 2 min, hold for 5 min; **B**) 1–6.7 % acetonitrile over 25 min, hold for 10 min, and then to 1% acetonitrile over 2 min, hold for 5 min.

Trapping of Covalent DNA—Peptide Complexes Using $NaCNBH_3$

The peptide KWKK was prepared by the National Institute of Environmental Health Sciences Center Protein Chemistry Laboratory at the University of Texas Medical Branch, Galveston, TX. Following initial synthesis, the peptide was analyzed by mass spectrometry, purified by preparative HPLC, and resuspended in a solution of 20:80 acetonitrile/water. The concentration of KWKK in solution was determined by monitoring Trp absorbance at 280 nm. The concentration was calculated using 5500 M^{-1} cm^{-1} as the Trp molar extinction coefficient. Adducted oligodeoxynucleotides (non-^{13}C or ^{15}N-isotopically labeled) were γ-^{32}P-labeled on the 5′ end with T4 polynucleotide kinase following standard procedures. For trapping reactions, adducted DNA (75 nM) was incubated with peptide in 100 mM HEPES (pH 7.0) and 100 mM NaCl at 4 °C. The concentrations of KWKK and $NaCNBH_3$ in trapping reactions were 1.0 mM and 50 mM, respectively, and reactions were quenched by the addition of 100 mM $NaBH_4$. (Aqueous solutions of both $NaCNBH_3$ and $NaBH_4$ were prepared fresh on the day of use.) Each reaction mixture was subsequently diluted 5-fold by the addition of 1.25× loading buffer (59 % v/v formamide, 12.5 mM EDTA, 0.012 % w/v bromophenol blue, 0.012 % xylene cyanol) and heated at 90°C for 3 min. The products of each reaction were separated on a 15% denaturing polyacrylamide gel (8.3 M urea) in sequencing buffer (134 mM Tris base, 44 mM boric acid, 10 mM EDTA) for 5 h at 1500 V. Results were visualized from wet gels by phosphorimager analysis, and product bands were quantitated using ImageQuant (5.0) software.

NMR

The isotopically labeled α-CH_3-γ-OH-PdG-modified oligodeoxynucleotide duplexes 5′-d(GCTAGCXAGTCC)-3′•5′-d(GGACTCYCTAGC)-3′ (X = α-CH_3-γ-OH-PdG; Y = dC, T, or dA) (Scheme 4) were annealed in a buffer consisting of 10 mM NaH_2PO_4, 0.1 M NaCl, and 50 μM Na_2EDTA (pH 7.0). The duplex oligodeoxynucleotides were eluted from DNA Grade Biogel hydroxylapatite (Bio-Rad Laboratories, Hercules, CA) with a gradient from 10 to 200 mM NaH_2PO_4 (pH 7.0). They were desalted using Sephadex G-25. The duplex oligodeoxynucleotides were prepared at a concentration of 1 mM in 0.3 mL of 9:1 H_2O:D_2O containing 10 mM NaH_2PO_4, 0.1 M NaCl, and 50 μM Na_2EDTA (pH 7.0). They were placed in micro-NMR tubes (Shigemi Glass, Inc., Allison Park, PA). NMR experiments were carried out at ^1H frequencies of 500.13 or 600.13 MHz (^{13}C frequencies of 125 or 150 MHz; ^{15}N frequencies of 50.66 or 60.79 MHz). One-dimensional ^{13}C NMR was conducted using a probe with inner-coil ^{13}C geometry using inverse-gated ^1H WALTZ16 decoupling. Typical acquisition parameters were 16 K total data points, with a digital resolution of 1.3 Hz/pt, 12K scans, and a relaxation delay of 8 s. ^{13}C HSQC experiments were performed using standard ^1H-detected pulse programs with States-TPPI phase cycling and watergate water suppression (32). Typical experimental parameters were 512 FIDs, each of 2K points. The ^{13}C sweep width was varied from 20 to 180 ppm. ^{15}N-HSQC spectra (33) were recorded with 8/180 scans per increment, using States-TPPI phase cycling, a delay time 1/2 $^1J_{N\text{-}H}$ of 5.56 ms, 1536 complex data points for 10,000 Hz in the acquisition dimension and 256 points in the indirect dimension, covering 10,136.8 Hz, centered at 100 ppm. A relaxation delay of 1.5 sec was used. Fully coupled and ^{15}N decoupled spectra were recording using the same parameters, leaving the ^{15}N decoupling off during the acquisition time of the coupled spectrum. TOCSY-HSQC experiments (34) were recorded applying States phase cycling, 60 ms isotropic mixing time applied with a 10 KHz dipsi spin lock pulse sequence optimized for a 90 Hz $^1J_{N\text{-}H}$ coupling. 1536 complex data points for 10000.0 Hz in the acquisition dimension and 128 points in the indirect dimension, covering 1000.0 Hz centered around 106 ppm were measured. A relaxation delay of 1.2 sec was used and ^{15}N was fully decoupled during the

acquisition time. NOESY-HSQC (34,35) experiments were recorded applying States phase cycling, 150 ms mixing time and were optimized for a 90 Hz $^{1}J_{N\text{-}H}$ coupling. 1536 complex data points for 10000.0 Hz in the acquisition dimension and 128 points in the indirect dimension, covering 1000.0 Hz centered at 106 ppm were measured. A relaxation delay of 1.5 sec was used and ^{15}N was fully decoupled during the acquisition time. ^{1}H chemical shifts were referenced to water. ^{13}C and ^{15}N chemical shifts were referenced indirectly (36–38). NMR data were processed on Silicon Graphics Octane workstations using the programs FELIX2000 (Accelrys, Inc., San Diego, CA) or NMRPipe (39).

Molecular modeling

Modeling was performed on Silicon Graphics Octane workstations using the program AMBER 8.0 (40). Classical B-DNA was used as a reference structure to create starting structures for potential energy minimization (41). Diastereomers at the γ-carbon of carbinolamine crosslink **5a** and pyrimidopurinone crosslink **7a** were constructed using the BUILDER module of INSIGHT II (Accelrys, Inc., San Diego, CA). The program ANTECHAMBER was used and the atom types were based on AMBER atom types for parameterization. RESP atomic charges were calculated using GAUSSIAN98 (42) and the Hartree-Fock 6-31G* basis set. The generalized Born model for solvent (43,44) was utilized for potential energy minimization. Potential energy minimization used the AMBER 8.0 force field.

Results

Site-Specific Synthesis of ^{13}C-Labeled *R*- and *S*-α-CH_3-γ-^{13}C-OH-PdG Oligodeoxynucleotides

Stereospecific synthesis of the ^{13}C-labeled adducted oligodeoxynucleotides was accomplished using the post-oligomerization strategy previously employed for related modified oligodeoxynucleotides (22,27,28). This involved the incorporation of an electrophilic base, 2-fluoro-O^6-(2-trimethylsilylethyl)-2′-deoxyinosine (31), into an oligodeoxynucleotide via the corresponding phosphoramidite, followed by displacement of the fluoro group by an amine analogue of the mutagen via a nucleophilic aromatic substitution reaction (Scheme 3). A vicinal diol unit was used as a surrogate for the aldehyde group (Scheme 2), which was cleaved with sodium periodate after the adduction reaction to give the desired modified oligodeoxynucleotide. A significant advantage of this strategy was that access to both stereoisomers **2a** and **2b** in the resulting adducted oligodeoxynucleotides **17a**, **17b** was obtained by individually reacting the (*R*) and (*S*)-stereoisomers of the amines **14a**, **14b** with the same oligodeoxynucleotide containing the 2-fluoroinosine base (**15**, Scheme 3).

The synthesis of the ^{13}C-labeled amino diols (**14a**, **14b**) is shown in Scheme 2. Commercially available (*S*)-2-amino-1-propanol **8b** was N-protected as the corresponding Boc derivative **9b**. The hydroxyl group was then converted to the mesylate and displaced with ^{13}C-labeled potassium cyanide to give nitrile **10b**. Reduction of the nitrile to the aldehyde (**11b**) was followed by Wittig methylenation to olefin **12b** in acceptable overall yield. Treatment of the olefin with osmium tetroxide gave diol **13b** as a mixture of stereoisomers. Since the diol was eventually cleaved to the aldehyde, the stereochemistry of the diol was of no consequence. Deprotection gave 4*S*-amino-pentane-1,2-diol (**14b**). The antipodal 4*R*-enantiomer **14a** was prepared by an identical sequence starting from commercially available (*R*)-2-amino-1-propanol.

Epimerization of *R*- and *S*-α-CH_3-γ-OH-PdG Oligodeoxynucleotide Adducts

The single stranded 5′-d(GCTAGCXAGTCC)-3′, modified with either the *R*- or *S*-α-CH_3-γ-OH-PdG adducts, was examined using ^{13}C HSQC NMR (Figure 1). At pH 7 and 15 °C, a single crosspeak was observed for *R*-α-CH_3-γ-OH-PdG adduct **2a**, at a ^{13}C chemical shift of 71.9

ppm, and a ^{1}H chemical shift of 5.96 ppm. This crosspeak was assigned as the epimer in which the α-CH_3 and γ-OH groups were in the *trans* configuration. For *S*-α-CH_3-γ-OH-PdG adduct **2b**, two crosspeaks were observed at pH 7 and 15 °C. The major crosspeak was observed at a ^{13}C chemical shift of 71.5 ppm, and a ^{1}H chemical shift of 5.89 ppm, also assigned as the epimer in which the α-CH_3 and γ-OH groups were in the *trans* configuration. The minor crosspeak was observed at a ^{13}C chemical shift of 71.6 ppm, and a ^{1}H chemical shift of 6.12 ppm. It was assigned as the hydroxyl epimer at the γ-carbon in which the α-CH_3 and γ-OH groups were in the *cis* configuration. In both instances, as temperature was increased to 37 °C, increasing amounts of the *cis* epimers appeared in the ^{13}C HSQC spectra, as measured by comparative volume integrations of the two resonances as a function of temperature. For *R*-α-CH_3-γ-OH-PdG adduct **2a**, the *cis* epimer crosspeak was observed at a ^{13}C chemical shift of 71.3 ppm, and a ^{1}H chemical shift of 6.10 ppm. No resonances for γ-^{13}C aldehydes **3a** or **3b**, or hydrated aldehydes **4a** or **4b** were observed, suggesting that at equilibrium, the levels of these ring-opened species remained below the spectroscopic limit of detection.

To detect the transient presence of aldehydes **3a** or **3b**, a series of peptide trapping experiments were performed. The single-stranded oligodeoxynucleotide 5′-d(GCTAGCXAGTCC)-3′ containing either a *R*- or *S*-α-CH_3-γ-OH-PdG adduct was treated with the peptide KWKK for 0–120 min in the presence of $NaCNBH_3$. Reaction mixtures were quenched at the designated time points by adding $NaBH_4$ to reduce the aldehyde substrate. A gel-shifted complex was observed by denaturing PAGE analysis and designated as DNA—peptide crosslink (Figure 2, 12-mer + KWKK), consistent with the transient presence of aldehydes **3a** or **3b** in single-stranded DNA. The accumulation of this product band was monitored over a 2 hr time course (Figure 2), at 4, 15, 37 or 50 °C. Higher temperatures facilitated faster formation of the peptide-DNA conjugate. At 4 °C, there was little complex accumulation over the 2 hr time course, whereas at 50 °C a substantial amount of complex accumulated over this time period. These results were consistent with the NMR data, in which the rate of epimerization of the *R*- or *S*-α-CH_3-γ-OH-PdG adducts increased at higher temperatures in single-stranded DNA.

On the ms time scale of the NMR experiments, the two epimers of the γ-hydroxyl groups of the of 1,N^2-dG adducts **2a** and **2b** were in slow exchange. A series of ^{13}C HSQC spectra collected as a function of temperature enabled van't Hoff analysis (Figure 3). These studies revealed that for the *R* adduct **2a**, the value of ΔH for the *cis* to *trans* interconversion was −14 kcal/mol and the value of ΔS for the interconversion was −42 cal/mol K. For the *S* adduct **2b**, the value of ΔH for the *cis* to *trans* interconversion was −10 kcal/mol and the value of ΔS for the interconversion was −29 cal/mol K.

Equilibrium Chemistry of the *R*-α-CH_3-γ-OH-PdG Adduct in Duplex DNA

The *R*- α-CH_3-γ-^{13}C-OH-PdG adduct **2a** was placed opposite dC in 5′-d(GCTAGCXAGTCC)-3′•5′-d(GGACTCGCTAGC)-3′ at pH 7, and the sample was allowed to equilibrate at 37 °C. An inverse-gated ^{13}C spectrum was obtained immediately upon annealing the duplex. The γ-^{13}C resonances from aldehyde **3a** and hydrated aldehyde **4a** were detected, indicating that opening of adduct **2a** occurred before the ^{13}C spectrum could be collected. At pH 7, opening of the crotonaldehyde-derived 1,N^2-dG adduct **2a** to aldehyde **3a** and hydrated aldehyde **4a** was incomplete. After 20 days, no further spectroscopic changes were observed. At equilibrium, the γ-^{13}C resonance appeared as a mixture of four species. Furthest downfield, at 208 ppm, was a resonance assigned as γ-^{13}C aldehyde **3a**. A second γ-^{13}C resonance, assigned as hydrated aldehyde **4a**, was observed at 90 ppm. The third resonance, identified as carbinolamine crosslink **5a**, was observed at 73 ppm. This resonance increased in intensity over a period of 20 days at 37 °C. The two γ-hydroxyl diastereomers of crosslink **5a** were not resolvable in the ^{13}C spectrum, but were resolved using ^{1}H and ^{15}N NMR, as will be discussed below. The failure to observe a γ-^{13}C resonance in the 140–160

ppm spectral region, the range in which a resonance arising from γ-^{13}C imine **6a** would be anticipated, indicated that the amount of imine **6a** in equilibrium with carbinolamine **5a** was below the level of detection by ^{13}C NMR. This placed an upper limit on the amount of 5′-CpG-3′ imine crosslink **6a** in equilibrium with carbinolamine crosslink **5a**, estimated to be ≤ 5%. A fourth resonance, assigned as cyclic adduct **2a**, was observed at 72 ppm. The ~1 ppm ^{13}C chemical shift difference of adduct **5a** as compared to adduct **2a** was consistent with the expectation that the γ-^{13}C nuclei in adducts **2a** and **5a**, both of which were bonded to hydroxyl groups, should exhibit similar chemical shifts.

Confirmation of the assignment of carbinolamine crosslink **5a** came from a series of ^{15}N-HSQC and ^{15}N-edited HSQC and NOESY experiments (Figure 5). The ^{15}N HSQC experiment revealed crosspeaks corresponding to the anticipated diastereomers of carbinolamine crosslink **5a**. The stronger of these two crosspeaks exhibited a ^{15}N chemical shift of 106 ppm and a ^{1}H chemical shift of 8.4 ppm. This crosspeak exhibited a 90 Hz coupling constant. The weaker of the two crosspeaks was observed at a ^{15}N chemical shift of 96 ppm and a ^{1}H chemical shift of 8.7 ppm. Two additional weaker crosspeaks in the ^{15}N-HSQC spectrum were assigned as arising from non-crosslinked oligodeoxynucleotide, in which $^{15}N^2$-dG-labeled base pair C^6•Y^{19} retained Watson-Crick hydrogen bonding. The crosspeak at 8.0 in the ^{1}H dimension was assigned as arising from the hydrogen bonded amino proton, whereas that at 6.5 in the ^{1}H dimension arose from the non-hydrogen bonded amino proton. An additional minor ^{15}N-HSQC, labeled as peak e in Figure 5a, remained unidentified.

The ^{15}N-HSQC-filtered TOCSY experiment (Figure 5) established that the ^{1}H signal at 8.35 ppm, assigned as Y^{19} N^2H in carbinolamine crosslink **5a**, exibited scalar coupling to protons of the crosslink crotonaldehyde moiety. The signal observed at 5.79 ppm indicated coupling to H_γ of the crotonaldehyde crosslink. Crosspeaks at 1.5 and 2.2 ppm were observed to the $H_{\beta',\beta''}$ crotonaldehyde protons. No crosspeaks were observed for the minor diastereomer of the carbinolamine crosslink, presumably due to its low abundance.

A ^{15}N HSQC-filtered NOESY experiment (Figure 5) revealed that for the major diastereomer of crosslink **5a**, the Y^{19} N^2H→Y^{19} N1H NOE was observed at 12.8 ppm, in the expected chemical shift range for this imino proton involved in Watson-Crick hydrogen bonding. For the major diastereomer, NOEs were observed from Y^{19} N^2H to H_α, $H_{\beta',\beta''}$, H_γ, and the methyl protons of the crotonaldehyde crosslink. For the minor diastereomer of crosslink **5a**, the Y^{19} N^2H→Y^{19} N1H NOE was observed at 13.0 ppm, also in the expected chemical shift range for a Watson-Crick hydrogen bonded imino proton.

The assignment of carbinolamine crosslink **5a** was corroborated by a triple resonance HNC experiment, in which the complementary strand of the duplex was site-specifically labeled with $^{15}N^2$-dG at the crosslinked dG residue (Figure 6). This experiment exploited the fact that crosslink formation resulted in bonding between the $^{15}N^2$-dG and γ-^{13}C isotopes. A correlation was observed between the 73 ppm γ-^{13}C resonance, and a ^{15}N resonance at 106 ppm, establishing that these resonances arose from the same chemical species observed in ^{15}N HSQC experiments, and assigned as carbinolamine **5a**. No correlation was observed between the signal arising from the minor diastereomer observed at 96 ppm in the ^{15}N HSQC spectrum, and ^{13}C, presumably because of the low abundance of the minor diastereomer of crosslink **5a** observed in the ^{15}NHSQC experiments.

Equilibrium Chemistry of the *S*-α-CH_3-γ-OH-PdG Adduct in Duplex DNA

The *S*-α-CH_3-γ-^{13}C-OH-PdG adduct differed from the *R*-α-CH_3-γ-^{13}C-OH-PdG adduct. At equilibrium, only low levels of interstrand crosslinks were observed in the 5′-CpG-3′ sequence, as demonstrated by reductive trapping with $NaCNBH_4$ (23). The *S*-α-CH_3-γ-^{13}C-OH-PdG adduct **2b** was placed opposite dC in 5′-d(GCTAGCXAGTCC)-3′•5′-d

(GGACTCGCTAGC)-3′ at pH 7 and 37°C, and an inverse-gated ^{13}C spectrum was obtained immediately upon annealing the duplex at 37 °C. Similar to the *R*-α-CH_3-γ-^{13}C-OH-PdG adduct, the γ-^{13}C resonances from aldehyde **3b** and hydrated aldehyde **4b** were detected. Thus, opening of cyclic adduct **2b** occurred before the ^{13}C spectrum could be collected. Also similar to the *R*-α-CH_3-γ-^{13}C-OH-PdG adduct, at pH 7, opening of crotonaldehyde-derived 1,N^2-dG adduct **2b** to aldehyde **3b** and hydrated aldehyde **4b** was incomplete. After 20 days, no further spectroscopic changes were observed. Both the *R*-α-CH_3-γ-^{13}C-OH-PdG and *S*-α-CH_3-γ-^{13}C-OH-PdG exhibited similar quantities of the 1,N^2-dG cyclic adducts **2a** or **2b** in equilibrium with aldehydes **3a** or **3b** and hydrated aldehydes **4a** or **4b**, suggesting that the positions of the equilibria involving the 1,N^2-dG adducts and their ring-opened rearrangement products were independent of stereochemistry at C_α of the crotonaldehyde moiety. Significantly, however, and corroborating the reductive trapping experiments (23), ^{13}C NMR failed to detect crosslink **5b**, confirming that formation of the interstrand crosslink in the 5′-CpG-3′ sequence was dependent upon stereochemistry at C_α of the crotonaldehyde moiety.

Figure 7 shows the ^{13}C NMR spectrum of the *S*-α-CH_3-γ-^{13}C-OH-PdG adduct **2b** when placed opposite dC in 5′-d(GCTAGCXAGTCC)-3′•5′-d(GGACTCGCTAGC)-3′ at 37 °C, at pH values of 4.7, 9.3, and 10.7. At pH 4.7, the equilibrium between 1,N^2-dG adduct **2b** and N^2-(3-oxopropyl)-dG aldehyde **3b** and its hydrate **4b** favored cyclic adduct **2b**. Increasing the pH to 9.3 favored formation of N^2-(3-oxopropyl)-dG aldehyde **3b** and its hydrate **4b**. At pH 10.7, denaturation of the oligodeoxynucleotide duplex occurred, and only cyclic adduct **2b** was observed.

Mispairing of T Opposite the γ-OH-PdG Adduct

Figure 8 shows the ^{13}C NMR spectrum of the *S*-α-CH_3-γ-^{13}C-OH-PdG adduct **2b** when placed opposite T in 5′-d(GCTAGCXAGTCC)-3′•5′-d(GGACTTGCTAGC)-3′ at 37 °C, at pH 7. Under these conditions, cyclic adduct **2a** was favored, with N^2-(3-oxopropyl)-dG aldehyde **3b** and its hydrate **4b** remaining below the level of detection by ^{13}C NMR.

Molecular Modeling

The two carbinolamine crosslinks **5a** and **5b** arising from interstrand crosslinking by adducts **2a** or **2b**, respectively, were modeled in 5′-d(GCTAGCXAGTCC)-3′•5′-d (GGACTCGCTAGC)-3′. The model structures were subjected to potential energy minimization using the conjugate gradients algorithm in AMBER 8.0 (Figure 9). The potential energy minimization predicted that for crosslink **5a**, arising from *R*-α-CH_3-γ-OH-PdG, the methyl group projected into the minor groove, without disruption of duplex DNA structure. In contrast, the calculations predicted that for crosslink **5b**, arising from *S*-α-CH_3-γ-OH-PdG, the methyl group interfered with the 3′-neighbor base pair A^8•T^{17}, presumably reducing the stability of the crosslinked duplex.

Additionally, the two N^2-(3-oxopropyl)-dG aldehydes **3a** and **3b** were modeled in 5′-d (GCTAGCXAGTCC)-3′•5′-d(GGACTCGCTAGC)-3′ and compared to the corresponding acrolein-derived N^2-(3-oxopropyl)-dG aldehyde, lacking the stereocenter at C_α of the N^2-(3-oxopropyl)-dG (Figure 10). The model structures were subjected to potential energy minimization using the conjugate gradients algorithm in AMBER 8.0. The potential energy minimization predicted that both N^2-(3-oxopropyl)-dG aldehydes **3a** and **3b** maintained Watson-Crick hydrogen bonding at both base pairs C^6•Y^{19} and X^7•C^{18} involved in the interstrand 5′-CpG-3′ crosslinks. The modeling studies suggested that for the *R*-stereoisomer of N^2-(3-oxopropyl)-dG aldehyde **3a**, the C_α methyl group oriented within the minor groove in the 3′-direction from the adducted nucleotide X^7. This oriented the reactive aldehyde group in the 5′-direction, placing it proximate to the crosslinking target N^2-dG in base pair C^6•Y^{19}. The favored orientation of the corresponding acrolein-derived N^2-(3-oxopropyl)-dG aldehyde

was similar, placing the aldehyde group in the 5′-direction, proximate to the crosslinking target N^2-dG in base pair C^6•Y^{19}. In contrast, the modeling studies suggested that the for the *S*-stereoisomer of N^2-(3-oxopropyl)-dG aldehyde **3b**, the C_α methyl group oriented within the minor groove in the 5′-direction from the adducted nucleotide X^7. This oriented the aldehyde group in the 3′-direction, placing it distal to the crosslinking target N^2-dG in base pair C^6•Y^{19}.

The two γ-hydroxyl diastereomers of the 5′-CpG-3′ carbinolamine crosslink **5a** arising from *R*-α-CH_3-γ-OH-PdG adduct **2a** were modeled and compared to the corresponding unmodified oligodeoxynucleotide sequence. The model structures were subjected to potential energy minimization using the conjugate gradients algorithm in AMBER 8.0 (Figure 11). The potential energy minimization predicted that both diastereomers of carbinolamine crosslink maintained Watson-Crick hydrogen bonding at both of the tandem C•G base pairs involved in the interstrand crosslinks. The modeling studies suggested that the sp^3 hybridization at the γ-carbon allowed the crosslinks to form without substantial perturbation of duplex structure. For the *S*-diastereomer of the carbinolamine crosslink, the molecular modeling predicted an additional hydrogen bond between the carbinolamine hydroxyl and N3-dG of the 5′ C•G base pair of the crosslink. In contrast, the imine in crosslink **6a** mandated sp^2 hybridization of the amino group, which would require breaking the Watson-Crick hydrogen bond between the amine proton of N^2-dG and O^2-dC of the 5′ C•G base pair in the crosslink. Formation of either diastereomer of pyrimidopurinone crosslink **7a** prevented Watson-Crick hydrogen bonding at the 3′ G•C base pair of the crosslink. It also disrupted Watson-Crick hydrogen bonding at the 5′ C•G base pair of the crosslink. The parameterization of the carbinolamine and the pyrimidopurinone crosslinks, for the AMBER 8.0 forcefield, is provided in Figure S1 of the Supporting Information.

Discussion

Epimerization of the Stereoisomeric *R*- and *S*-α-CH_3-γ-OH-PdG Adducts in the 5′-CpG-3′ Sequence

At equilibrium in single-stranded DNA, the *R*- and *S*-α-CH_3-γ-OH-PdG adducts **2a** and **2b** existed as mixtures of epimers of the 1,N^2-dG adduct at C_γ, in slow exchange on the NMR time scale. In both instances, the *trans* orientation of the α-CH_3 and γ-OH groups predominated. This observation was consistent with previous observations in the NMR spectra of the nucleosides (45,46). This differed from the acrolein-derived γ-OH-PdG adduct lacking the CH_3 group at C_α, which exhibited equal amounts of both epimers.

The failure to observe a γ-^{13}C resonance corresponding to ring-opened aldehydes **3a** or **3b** in single-stranded DNA was consistent with the observation that at pH 7, cyclic adducts **2a** or **2b** were favored as compared to ring-opened aldehydes **3a** or **3b**. The NMR data suggested that in single-stranded DNA, adducts **2a** and **2b** spontaneously epimerized, but slowly on the NMR time scale, without accumulation of aldehydes **3a** or **3b**. Nevertheless, the peptide trapping data revealed the transient presence of the aldehydes **3a** or **3b** (Figure 2).

Ring Opening of the *R*- and *S*-α-CH_3-γ-OH-PdG Adducts in Duplex DNA in the 5′-CpG-3′ Sequence

For both the *R*- and *S*-α-CH_3-γ-OH-PdG adducts the presence of duplex DNA was required for the stable formation of the aldehydes **3a** and **3b**, as observed for the acrolein-derived γ-HOPdG adduct (21). In duplex DNA, the aldehydes **3a** or **3b**, and their hydrates **4a** or **4b**, similar to the acrolein γ-OH-PdG adduct (21) and the malondialdehyde M_1dG adduct (47, 48), are accommodated in the minor groove of DNA, enabling maintenance of Watson-Crick hydrogen bonding at the adducted base pair. Significantly, in comparing the chemistry of the

R- and *S*-α-CH_3-γ-OH-PdG adducts **2a** and **2b** when placed into duplex DNA opposite dC at pH 7 with the corresponding acrolein-derived γ-OH-PdG adduct (21), ring-opening of the *R*- and *S*-α-CH_3-γ-OH-PdG adducts **2a** and **2b** to the aldehydes **3a** and **3b** and the hydrated aldehydes **4a** and **4b** was incomplete. When the acrolein γ-OH-PdG adduct was placed opposite dC in duplex DNA, equilibrium favored the ring-opened N^2-(3-oxopropyl)-dG aldehyde and its hydrate, to the extent that the 1,N^2-dG adduct was no longer detected (21). The incomplete opening of the *R*- and *S*-α-CH_3-γ-OH-PdG adducts **2a** and **2b** in duplex DNA, when placed opposite dC, might be explained by the fact that cyclic adducts **2a** and **2b** position the CH_3 groups to avoid steric clash with N3 of the guanine. This becomes an issue upon formation of the N^2-(3-oxopropyl)-dG aldehydes **3a** and **3b**. The stabilization of cyclic adducts **2a** and **2b** might also arise from the Thorpe-Ingold effect. For the *R*- and *S*-α-CH_3-γ-OH-PdG adducts **2a** and **2b** in duplex DNA, the degree to which the 1,N^2-dG adducts opened to the N^2-(3-oxopropyl)-dG aldehydes **3a** and **3b** increased significantly at pH 9.3 (Figure 7). In duplex DNA at pH 7, crosslinks formed between the N-terminal peptide amine and the aldehyde rearrangement products **3a** and **3b** of the *R*- and *S*-α-CH_3-γ-OH-PdG adducts at 4 °C (26).

One factor with regard to the ring opening of adduct **2b** to aldehyde **3b** in duplex DNA was the identity of the nucleotide opposite the 1,N^2-dG adduct. When placed opposite to T in duplex DNA, the *S*-α-CH_3-γ-OH-PdG adduct did not undergo ring-opening to aldehyde **3b** (Figure 8), whereas the acrolein-derived γ-OH-PdG adduct when mispaired with T, existed as a mixture of the 1,N^2-dG adduct and the ring-opened aldehyde (25). When mispaired with T, the M_1dG adduct remained as the 1,N^2-dG adduct (47). Similar to the acrolein-derived γ-OH-PdG adduct, the ratio of aldehyde to hydrated aldehyde (**3a:4a** or **3b:4b**) for the crotonaldehyde-derived adducts increased with temperature.

Role of Stereochemistry in Interstrand Crosslinking in the 5′-CpG-3′ Sequence Context

The presence of aldehydes **3a** or **3b** in the minor groove at pH 7 and 37 °C was significant with regard to their potential for forming interstrand crosslinks **5a** or **5b** under physiological conditions in the 5′-CpG-3′ sequence. The present NMR studies corroborate the stereospecific preference for DNA interstrand crosslinking by the *R*-α-CH_3-γ-OH-PdG adduct, as opposed to the *S*-α-CH_3-γ-OH-PdG adduct (23). The time required for crosslink **5a** to reach equilibrium at pH 7 and 37 °C was approximately 20 days, with approximately 26% crosslinking observed.

To examine why interstrand crosslinking was much more extensive for the *R*-α-CH_3-γ-^{13}C-OH-PdG adduct **2a** than for the *S*-α-CH_3-γ-^{13}C-OH-PdG adduct **2b** in the 5′-CpG-3′ sequence context, a molecular modeling approach was employed (Figure 9). The modeling studies suggested that the low levels of crosslinking observed for the *S*-α-CH_3-γ-^{13}C-OH-PdG adduct **2b** in the 5′-CpG-3′ sequence might be attributed to the fact that the carbinolamine crosslink **5b** was of lower stability than that of crosslink **5a**, presumably due to the differential orientation of the CH_3 group at the α-carbon of the crosslink. Anecdotally, Lao and Hecht reported conducting molecular dynamics studies of pyrimidopurinone crosslinks **7a** and **7b**, formed from adducts **2a** and **2b**, respectively, and reaching a similar conclusion, i.e., that the pyrimidopurinone crosslink arising from the *R*-α-CH_3-γ-^{13}C-OH-PdG adduct **2a** was of greater stability, due to a more favorable orientation of the α-carbon methyl group within the minor groove (10). The modeling studies also suggested that aldehyde **3b**, arising from adduct **2b** in duplex DNA, would not be oriented favorably for reaction with the crosslinking target N^2-dG in base pair C^6•Y^{19}; thus the rate of formation of the crosslink arising from aldehyde **3b** would be expected to be slower (Figure 10). NMR studies designed to examine these structural hypotheses are in progress.

Formation of an Interstrand Carbinolamine Crosslink by the *R*-α-CH_3-γ-OH-PdG Adduct

At equilibrium in duplex DNA, the interstrand *R*-α-CH_3-γ-OH-PdG crosslink is comprised of a mixture of carbinolamine **5a**, imine **6a**, and pyrimidopurinone **7a**. The presence of some of imine **6a** was inferred since the crosslink was reductively trapped in the presence of $NaCNBH_3$ (23). Lao and Hecht, using negative ion mode ESI-Q-TOF-MS analysis of a crosslinked oligodeoxynucleotide, observed *m/z* values corresponding to carbinolamine **5a** and either imine **6a** or pyrimidopurinone **7a**, with the lower *m/z* signal corresponding to imine **6a** or pyrimidopurinone **7a** predominating (10). The present NMR studies suggested that the predominant form of the *R*-α-CH_3-γ-OH-PdG crosslink *in situ*, is not imine **6a**. The amount of imine **6a** remained below the level of spectroscopic detection in duplex DNA. The reduction of crosslinked imine **6a** was slow in the presence of $NaCNBH_3$ (23), consistent with the notion that conversion of carbinolamine **5a** to the reducible imine **6a** was rate limiting in reductively trapping the crosslink in duplex DNA.

Similar to the acrolein-derived γ-OH-PdG interstrand crosslink (25), molecular modeling revealed that the carbinolamine linkage of crosslink **5a** maintained Watson-Crick hydrogen bonding at both of the tandem C•G base pairs (Figure 11). In contrast, dehydration of the carbinolamine crosslink to imine (Schiff base) crosslink **6a**, or cyclization of the latter to form pyrimidopurinone crosslink **7a**, required disruption of Watson-Crick hydrogen bonding at one or both of the tandem crosslinked C•G base pairs. The NMR studies supported this conclusion, suggesting intact Watson-Crick base pairing at the crosslinked X^7•C^{18} (Figure 5). In contrast, enzymatic digestion of duplex DNA containing crosslink **5a** afforded a bis-deoxyguanosine conjugate, characterized by a combination of mass spectrometry and NMR as pyrimidopurinone **7a** arising from annelation of imine **6a** with N1-dG in the 5′-Cp<u>G</u>-3′ sequence (23). The likely explanation is that the equilibrium between carbinolamine **5a**, imine **6a**, and pyrimidopurinone **7a** depends upon the conformational state of the DNA. Enzymatic degradation of duplex DNA favors collapse of the carbinolamine crosslink **5a** to the pyrimidopurinone bis-nucleoside crosslink **7a**.

Structure-Biological Activity Relationships

Site specific mutagenesis in COS-7 mammalian cells using the single-stranded pMS2 shuttle vector (49) indicated that both the *R*- and *S*-α-CH_3-γ-OH-PdG adducts yielded mutations at a 5–6% frequency. These were predominantly G→T transversions, corroborating experiments utilizing a randomly modified shuttle vector and replicated in human cells (50). In the same mammalian site-specific mutagenesis system, the acrolein-derived γ-OH-PdG adduct showed a greater frequency of mutations also predominantly G→T mutations (51). The propensity of cyclic adducts **2a** or **2b** to undergo ring opening to the N^2-(3-oxopropyl)-dG aldehydes **3a** or **3b** may facilitate lesion bypass, as reported for the acrolein-derived γ-OH-PdG adduct (52–56). On the other hand, in duplex DNA, incomplete conversion of crotonaldehyde-derived adducts **2a** and **2b** to the aldehydes **3a** and **3b** or hydrated aldehydes **4a** and **4b** may result in a more efficient block to DNA replication, possibly reducing their mutagenicity. The *R*- and *S*-α-CH_3-γ-OH-PdG adducts were reported to block trans-lesion synthesis by the Klenow (*exo*-) fragment of DNA polymerase I and DNA polymerase ε (57). The enzymes responsible for trans-lesion synthesis of the *R*- and *S*-α-CH_3-γ-OH-PdG adducts remain to be identified. However, Washington et al. (58,59) showed that the Y-polymerase pol ι in conjunction with pol κ or Rev 1 in combination with pol ζ could efficiently bypass the acrolein-derived γ-OH-PdG adduct. Minko et al. showed that pol η could bypass the γ-OH-PdG to a lesser extent (60). It seems plausible that these error-prone polymerases might also bypass the *R*- and *S*-α-CH_3-γ-OH-PdG adducts.

Summary

The chemistry of the *R*- and *S*-α-CH_3-γ-OH-PdG adducts in DNA was similar to that of the acrolein-derived γ-OH-PdG adducts, but the positions of chemical equilibria differed. At pH 7 in single-stranded DNA only the 1,N^2-dG adducts **2a** and **2b** were observed. The epimers having *trans* configuration of the α-CH_3 and γ-OH groups were favored. The transient presence of ring-opened aldehydes **3a** and **3b** was established by peptide trapping experiments. When placed opposite dC in duplex DNA at pH 7, the *R*- and *S*-α-CH_3-γ-OH-PdG adducts **2a** and **2b** did not completely convert to ring-opened aldehydes. When the *S*-α-CH_3-γ-OH-PdG adduct **2b** was placed opposite T, only the 1, N^2-dG adduct was observed. Interstrand crosslinking in the 5′-CpG-3′ sequence was observed spectroscopically only for the *R*-α-CH_3-γ-OH-PdG adduct, corroborating results of reductive trapping experiments (23). Molecular modeling predicted that carbinolamine **5a** arising from adduct **2a** should be favored as compared to carbinolamine **5b** arising from adduct **2b**. It also predicted that the aldehyde rearrangement product **3a** of the *R*-α-CH_3-γ-OH-PdG adduct **2a** was oriented in the minor groove with the aldehyde moiety in the 5′-direction, potentially facilitating crosslinking with N^2-dG in the complementary strand of the 5′-CpX-3′ sequence, whereas for the *S*-α-CH_3-γ-OH-PdG adduct **2b**, the aldehyde moiety oriented in the minor groove in the 3′-direction, hindering crosslinking. Similar to the γ-OH-PdG crosslink, the interstrand crosslink formed in the 5′-CpG-3′ sequence existed predominantly as the carbinolamine **5a**.

Supplementary Material

Refer to Web version on PubMed Central for supplementary material.

Acknowledgements

We thank Ms. Pamela Tamura and Ms. Albena Kozekova for assistance with oligodeoxynucleotide synthesis and purification. This work was supported by NIH grant ES-05335 (T.M.H., R.S.L., C.J.R., and M.P.S). A.J.K. received support from NIH training grant ES-07254. Funding for the NMR spectrometers was supplied by Vanderbilt University; by NIH grant RR-05805, and the Vanderbilt Center in Molecular Toxicology, ES-00267. The Vanderbilt-Ingram Cancer Center is supported by NIH grant CA-68485. Peptide synthesis was supported by a NIH Center Grant to UTMB, ES-06676.

References

1. Czerny C, Eder E, Runger TM. Genotoxicity and mutagenicity of the α,β-unsaturated carbonyl compound crotonaldehyde (butenal) on a plasmid shuttle vector. Mutat. Res 1998;407:125–134. [PubMed: 9637241]
2. Chung FL, Tanaka T, Hecht SS. Induction of liver tumors in F344 rats by crotonaldehyde. Cancer Res 1986;46:1285–1289. [PubMed: 3002613]
3. Chung FL, Hecht SS. Formation of cyclic 1,N^2--adducts by reaction of deoxyguanosine with alpha-acetoxy-N-nitrosopyrrolidine, 4-(carbethoxynitrosamino)butanal, or crotonaldehyde. Cancer Res 1983;43:1230–1235. [PubMed: 6825094]
4. Eder E, Schuler D, Budiawan. Cancer risk assessment for crotonaldehyde and 2-hexenal: an approach. IARC Sci. Publ 1999;150:219–232. [PubMed: 10626223]
5. Chung FL, Zhang L, Ocando JE, Nath RG. Role of 1,N^2-propanodeoxyguanosine adducts as endogenous DNA lesions in rodents and humans. IARC Sci. Publ 1999;150:45–54. [PubMed: 10626207]
6. Wang M, McIntee EJ, Cheng G, Shi Y, Villalta PW, Hecht SS. Identification of DNA adducts of acetaldehyde. Chem. Res. Toxicol 2000;13:1149–1157. [PubMed: 11087437]
7. Wang M, McIntee EJ, Cheng G, Shi Y, Villalta PW, Hecht SS. Identification of paraldol-deoxyguanosine adducts in DNA reacted with crotonaldehyde. Chem. Res. Toxicol 2000;13:1065–1074. [PubMed: 11080056]

8. Wang M, McIntee EJ, Cheng G, Shi Y, Villalta PW, Hecht SS. A Schiff base is a major DNA adduct of crotonaldehyde. Chem. Res. Toxicol 2001;14:423–430. [PubMed: 11304131]
9. International Agency for Research on Cancer. Re-evaluation of some organic chemicals, hydrazine and hydrogen peroxide, IARC Monographs on the Evaluation of Carcinogenic Risks to Humans. IARC Sci. Publ 1999;71:109–125.
10. Lao Y, Hecht SS. Synthesis and properties of an acetaldehyde-derived oligonucleotide interstrand cross-link. Chem. Res. Toxicol 2005;18:711–721. [PubMed: 15833031]
11. Chung FL, Nath RG, Nagao M, Nishikawa A, Zhou GD, Randerath K. Endogenous formation and significance of 1,N^2-propanodeoxyguanosine adducts. Mutat. Res 1999;424:71–81. [PubMed: 10064851]
12. Budiawan, Eder E. Detection of 1,N^2-propanodeoxyguanosine adducts in DNA of Fischer 344 rats by an adapted ^{32}P-post-labeling technique after per os application of crotonaldehyde. Carcinogenesis 2000;21:1191–1196. [PubMed: 10837009]
13. Nath RG, Chung FL. Detection of exocyclic 1,N^2-propanodeoxyguanosine adducts as common DNA lesions in rodents and humans. Proc. Natl. Acad. Sci. USA 1994;91:7491–7495. [PubMed: 8052609]
14. Nath RG, Ocando JE, Chung FL. Detection of 1,N^2-propanodeoxyguanosine adducts as potential endogenous DNA lesions in rodent and human tissues. Cancer Res 1996;56:452–456. [PubMed: 8564951]
15. Treitman RD, Burgess WA, Gold A. Air contaminants encountered by firefighters. Am. Ind. Hyg. Assoc. J 1980;41:796–802. [PubMed: 7457369]
16. Izard C, Valadaud-Barrieu D, Fayeulle JP, Testa A. Effect of smoking-machine parameters on the genetoxic activity of cigarette gas phase, estimated on human lymphocyte and yeast (author's transl). Mutat. Res 1980;77:341–344. [PubMed: 6990251]
17. Chung FL, Chen HJ, Nath RG. Lipid peroxidation as a potential endogenous source for the formation of exocyclic DNA adducts. Carcinogenesis 1996;17:2105–2111. [PubMed: 8895475]
18. Hecht SS, Upadhyaya P, Wang M. Reactions of alpha-acetoxy-N-nitrosopyrrolidine and crotonaldehyde with DNA. IARC Sci. Publ 1999;150:147–154. [PubMed: 10626216]
19. Chung FL, Young R, Hecht SS. Formation of cyclic 1,N^2-propanodeoxyguanosine adducts in DNA upon reaction with acrolein or crotonaldehyde. Cancer Res 1984;44:990–995. [PubMed: 6318992]
20. Nath RG, Chen HJ, Nishikawa A, Young-Sciame R, Chung FL. A ^{32}P-postlabeling method for simultaneous detection and quantification of exocyclic etheno and propano adducts in DNA. Carcinogenesis 1994;15:979–984. [PubMed: 8200104]
21. de los Santos C, Zaliznyak T, Johnson F. NMR characterization of a DNA duplex containing the major acrolein-derived deoxyguanosine adduct γ-OH-1,-N^2-propano-2'-deoxyguanosine. J. Biol. Chem 2001;276:9077–9082. [PubMed: 11054428]
22. Kozekov ID, Nechev LV, Sanchez A, Harris CM, Lloyd RS, Harris TM. Interchain cross-linking of DNA mediated by the principal adduct of acrolein. Chem. Res. Toxicol 2001;14:1482–1485. [PubMed: 11712904]
23. Kozekov ID, Nechev LV, Moseley MS, Harris CM, Rizzo CJ, Stone MP, Harris TM. DNA interchain cross-links formed by acrolein and crotonaldehyde. J. Am. Chem. Soc 2003;125:50–61. [PubMed: 12515506]
24. Kim HY, Voehler M, Harris TM, Stone MP. Detection of an interchain carbinolamine cross-link formed in a CpG sequence by the acrolein DNA adduct γ-OH-1,N^2-propano-2′-deoxyguanosine. J. Am. Chem. Soc 2002;124:9324–9325. [PubMed: 12166998]
25. Cho Y-J, Kim H-Y, Huang H, Slutzky A, Minko IG, Wang H, Nechev LV, Kozekov ID, Kozekova A, Tamura P, Jacob J, Voehler M, Harris TM, Lloyd RS, Rizzo CJ, Stone M. Spectroscopic characterization of interstrand carbinolamine crosslinks formed in the 5′-CpG-3′ sequence by the acrolein-derived γ-OH-1,N^2-propano-2′-deoxyguanosine DNA adduct. J. Am. Chem. Soc 2005;127in press
26. Kurtz AJ, Lloyd RS. 1,N^2-deoxyguanosine adducts of acrolein, crotonaldehyde, and trans-4-hydroxynonenal cross-link to peptides via Schiff base linkage. J. Biol. Chem 2003;278:5970–5976. [PubMed: 12502710]

27. Nechev LV, Kozekov I, Harris CM, Harris TM. Stereospecific synthesis of oligonucleotides containing crotonaldehyde adducts of deoxyguanosine. Chem. Res. Toxicol 2001;14:1506–1512. [PubMed: 11712908]
28. Nechev LV, Zhang M, Tsarouhtsis D, Tamura PJ, Wilkinson AS, Harris CM, Harris TM. Synthesis and characterization of nucleosides and oligonucleotides bearing adducts of butadiene epoxides on adenine N^6 and guanine N^2. Chem. Res. Toxicol 2001;14:379–388. [PubMed: 11304126]
29. Borer, PN. Handbook of Biochemistry and Molecular Biology. Cleveland: CRC Press; 1975.
30. Harris CM, Zhou L, Strand EA, Harris TM. A new strategy for the synthesis of oligodeoxynucleotides bearing adducts at exocyclic amino sites of purine nucleosides. J. Am. Chem. Soc 1991;113:4328–4329.
31. DeCorte BL, Tsarouhtsis D, Kuchimanchi S, Cooper MD, Horton P, Harris CM, Harris TM. Improved strategies for postoligomerization synthesis of oligodeoxynucleotides bearing structurally defined adducts at the N^2 Position of deoxyguanosine. Chem. Res. Toxicol 1996;9:630–637. [PubMed: 8728509]
32. Piotto M, Saudek V, Sklenar V. Gradient-tailored excitation for single-quantum NMR spectroscopy of aqueous solutions. J. Biomol. NMR 1992;2:661–665. [PubMed: 1490109]
33. Sklenar V, Piotto M, Leppik RaSV. Gradient-tailored water suppression for ^{1}H-^{15}N HSQC Experiments optimized to retain full sensitivity. J. Magn. Reson 1993;102:241–245.
34. Talluri S, Wagner G. An optimized 3D NOESY-HSQC. J. Magn. Reson 1996;112:200–205.
35. Mori S, Abeygunawardana C, Johnson M, vanZul PCM. Improved sensitivity of HSQC spectra of exchanging protons at short interscan delays using a new fast HSQC (FHSQC) detection scheme that avoids water saturation. J. Magn. Reson 1995;108:94–98.
36. Markley JL, Bax A, Arata Y, Hilbers CW, Kaptein R, Sykes BD, Wright PE, Wuthrich K. Recommendations for the presentation of NMR structures of proteins and nucleic acids. J. Mol. Biol 1998;280:933–952. [PubMed: 9671561]
37. Wishart DS, Bigam CG, Yao J, Abildgaard F, Dyson HJ, Oldfield E, Markley JL, Sykes BD. ^{1}H, ^{13}C and ^{15}N chemical shift referencing in biomolecular NMR. J. Biomol. NMR 1995;6:135–140. [PubMed: 8589602]
38. International Union of Pure and Applied Chemistry. Recommendations for the presentation of NMR structures of proteins and nucleic acids. Pure Appl. Chem 1998;70:117–142.
39. Delaglio F, Grzesiek S, Vuister GW, Zhu G, Pfeifer J, Bax A. NMRPipe: A multidimensional spectral processing system based on UNIX pipes. J. Biomol. NMR 1995;6:277–293. [PubMed: 8520220]
40. Case, DA.; Darden, TA.; Cheatham, TE., III; Simmerling, CL.; Wang, J.; Duke, RE.; Luo, R.; Merz, KM.; Wang, B.; Pearlman, DA.; Crowley, M.; Brozell, S.; Tsui, V.; Gohlke, H.; Mongan, J.; Hornak, V.; Cui, G.; Beroza, P.; Schafmeister, C.; Caldwell, JW.; Ross, WS.; Kollman, PA. AMBER 8. San Francisco: University of California; 2004.
41. Arnott S, Hukins DWL. Optimised parameters for A-DNA and B-DNA. Biochem. Biophys. Res. Comm 1972;47:1504–1509. [PubMed: 5040245]
42. Frisch, MJ.; Trucks, GW., et al. GAUSSIAN 98. Pittsburgh, PA: Gaussian, Inc.; 1998.
43. Tsui V, Case DA. Theory and applications of the generalized Born solvation model in macromolecular simulations. Biopolymers 2000;56:275–291. [PubMed: 11754341]
44. Bashford D, Case DA. Generalized born models of macromolecular solvation effects. Annu. Rev. Phys. Chem 2000;51:129–152. [PubMed: 11031278]
45. Eder E, Hoffman C. Identification and characterization of deoxyguanosine-crotonaldehyde adducts. Formation of 7,8 cyclic adducts and 1,N^2,7,8 bis-cyclic adducts. Chem. Res. Toxicol 1992;5:802–808. [PubMed: 1489932]
46. Eder E, Hoffman C. Identification and characterization of deoxyguanosine adducts of mutagenic beta-alkyl-substituted acrolein congeners. Chem. Res. Toxicol 1993;6:486–494. [PubMed: 8374046]
47. Mao H, Schnetz-Boutaud NC, Weisenseel JP, Marnett LJ, Stone MP. Duplex DNA catalyzes the chemical rearrangement of a malondialdehyde deoxyguanosine adduct. Proc. Natl. Acad. Sci. USA 1999;96:6615–6620. [PubMed: 10359760]
48. Mao H, Reddy GR, Marnett LJ, Stone MP. Solution structure of an oligodeoxynucleotide containing the malondialdehyde deoxyguanosine adduct N^2-(3-oxo-1-propenyl)-dG (ring-opened M_1G)

positioned in a $(CpG)_3$ frameshift hotspot of the *Salmonella typhimurium hisD3052* gene. Biochemistry 1999;38:13491–13501. [PubMed: 10521256]

49. Moriya M. Single-stranded shuttle phagemid for mutagenesis studies in mammalian cells: 8-Oxoguanine in DNA induces targeted G:C-->T:A transversions in simian kidney cells. Proc. Natl. Acad. Sci. USA 1993;90:1122–1126. [PubMed: 8430083]
50. Kawanishi M, Matsuda T, Nakayama A, Takebe H, Matsui S, Yagi T. Molecular analysis of mutations induced by acrolein in human fibroblast cells using supF shuttle vector plasmids. Mutat. Res 1998;417:65–73. [PubMed: 9733921]
51. Kanuri M, Minko IG, Nechev LV, Harris TM, Harris CM, Lloyd RS. Error prone translesion synthesis past gamma-hydroxypropano deoxyguanosine, the primary acrolein-derived adduct in mammalian cells. J. Biol. Chem 2002;277:18257–18265. [PubMed: 11889127]
52. Yang IY, Hossain M, Miller H, Khullar S, Johnson F, Grollman A, Moriya M. Responses to the major acrolein-derived deoxyguanosine adduct in *Escherichia coli*. J. Biol. Chem 2001;276:9071–9076. [PubMed: 11124950]
53. Yang IY, Chan G, Miller H, Huang Y, Torres MC, Johnson F, Moriya M. Mutagenesis by acrolein-derived propanodeoxyguanosine adducts in human cells. Biochemistry 2002;41:13826–13832. [PubMed: 12427046]
54. Yang I-Y, Johnson R, Grollman AP, Moriya M. Genotoxic mechanism for the major acrolein-derived deoxyguanosine adduct in human cells. Chem. Res. Toxicol 2002;15:160–164. [PubMed: 11849041]
55. Sanchez A, Minko I, Kurtz AJ, Kanuri M, Moriya M, Lloyd RS. Comparative evaluation of the bioreactivity and mutagenic spectra of acrolein-derived _-HOPdG and _-HOPdG regioisomeric deoxyguanosine adducts. Chem. Res. Toxicol 2003;16:1019–1028. [PubMed: 12924930]
56. VanderVeen LA, Hashim MF, Nechev LV, Harris TM, Harris CM, Marnett LJ. Evaluation of the mutagenic potential of the principal DNA adduct of acrolein. J. Biol. Chem 2001;276:9066–9070. [PubMed: 11106660]
57. Fernandes PH, Kanuri M, Nechev LV, Harris TM, Lloyd RS. Mammalian cell mutagenesis of the DNA adducts of vinyl chloride and crotonaldehyde. Environ. Mol. Mutagen 2005;45:455–459. [PubMed: 15690339]
58. Washington MT, Minko IG, Johnson RE, Haracska L, Harris TM, Lloyd RS, Prakash S, Prakash L. Efficient and error-free replication past a minor-groove N^2-guanine adduct by the sequential action of yeast Rev1 and DNA polymerase zeta. Mol. Cell. Biol 2004;24:6900–6906. [PubMed: 15282292]
59. Washington MT, Minko IG, Johnson RE, Wolfle WT, Harris TM, Lloyd RS, Prakash S, Prakash L. Efficient and error-free replication past a minor-groove DNA adduct by the sequential action of human DNA polymerases iota and kappa. Mol. Cell. Biol 2004;24:5687–5693. [PubMed: 15199127]
60. Minko IG, Washington MT, Kanuri M, Prakash L, Prakash S, Lloyd RS. Translesion synthesis past acrolein-derived DNA adduct, γ-hydroxypropanodeoxyguanosine, by yeast and human DNA polymerase eta. J. Biol. Chem 2003;278:784–790. [PubMed: 12401796]

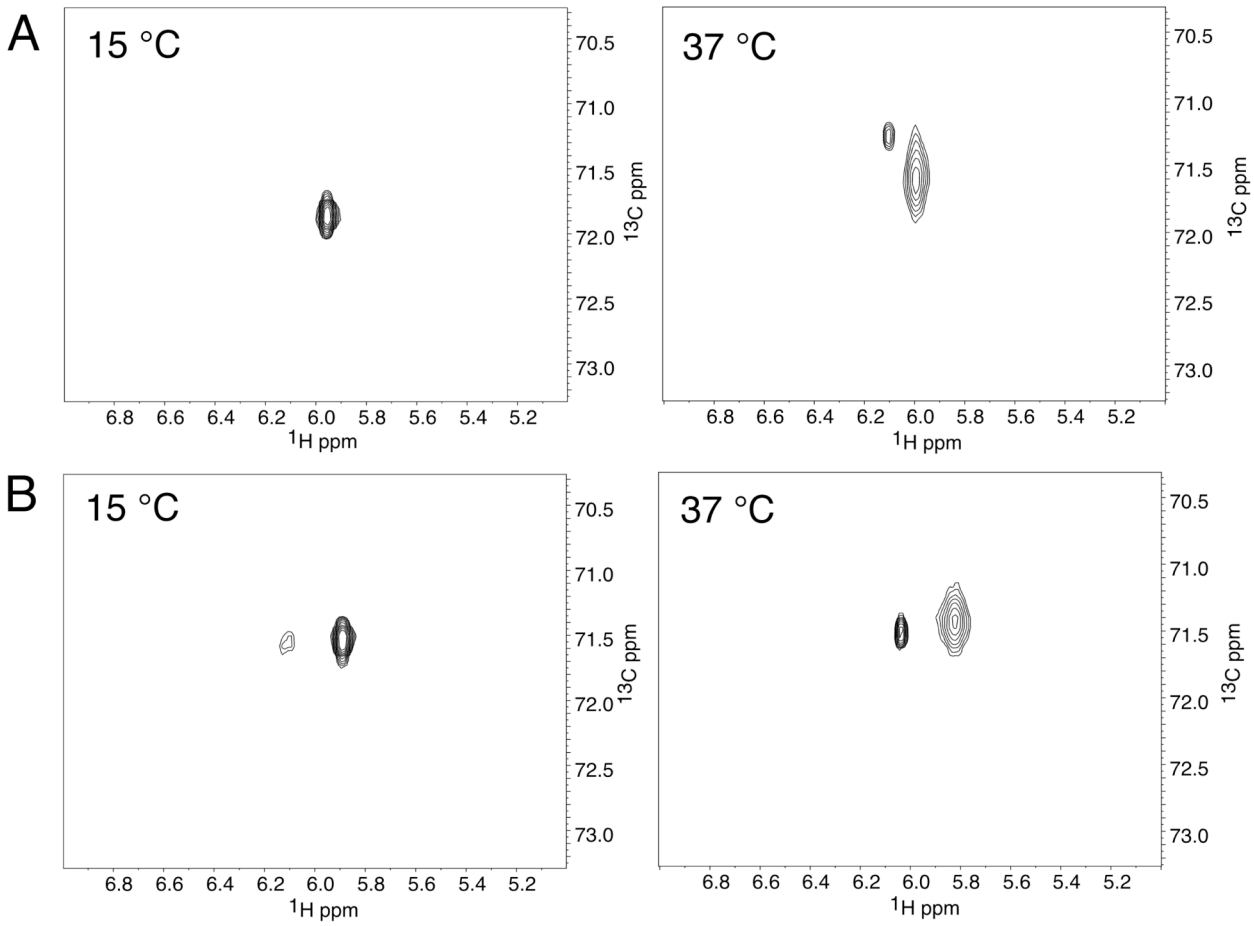

Figure 1.

^{13}C HSQC spectra of *R*- and *S*-α-CH_3-γ-OH-PdG adducts **2a** and **2b** in the oligodeoxynucleotide 5′-d(GCTAGCXAGTCC)-3′ at 15° and 37° C. **A.** *R*-α-CH_3-γ-OH-PdG, adduct **2a. B.** *S*-α-CH_3-γ-OH-PdG, adduct **2b**.

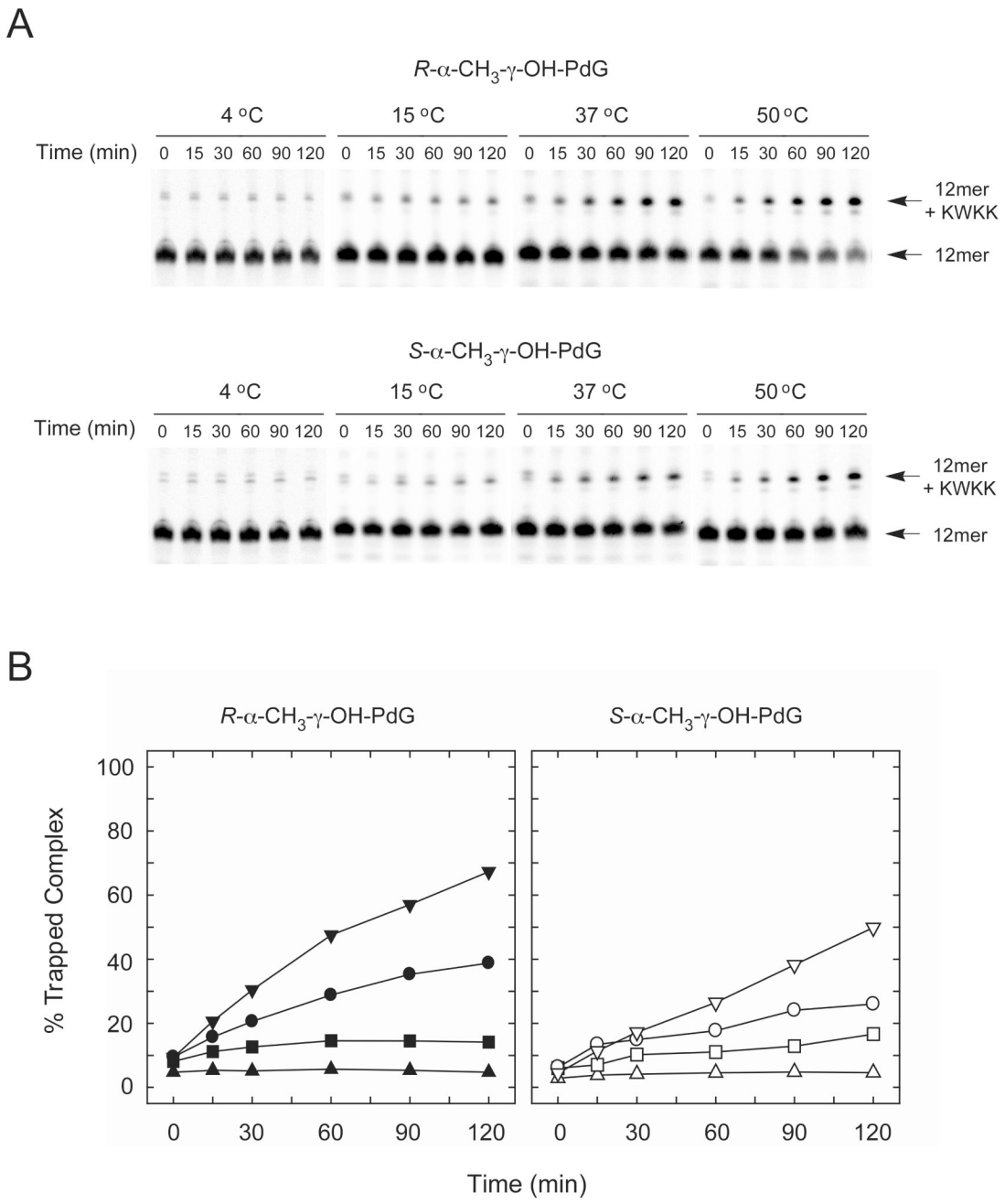

Figure 2.

DNA-peptide crosslinking involving *R*- and *S*-α-CH_3-γ-OH-PdG adducts. **A.** For trapping reactions, single-stranded crotonaldehyde-adducted oligodeoxynucleotides (75 nM) were incubated with 1.0 mM KWKK the presence of 50 mM $NaCNBH_3$ at 4, 15, 37 or 50 °C. Reactions were carried out in 100 mM HEPES (pH 7.0) and 100 mM NaCl and were incubated for 0, 15, 30, 60, 90 or 120 min. Reactions were quenched at the end of the incubation period by the addition of 100 mM $NaBH_4$. Labels indicate the positions of the substrate 12-mer DNAs and the major reduced Schiff base conjugates (12-mer + peptide) following denaturing PAGE analysis. **B.** Kinetics of trapped conjugate formation are plotted over the 2 h time course at 4 °C [*R*-α-CH_3-γ-OH-PdG, π; *S*-α-CH_3-γ-OH-PdG, ρ], 15 °C [*R*-α-CH_3-γ-OH-PdG, ´; *S*-α-

CH_3-γ-OH-PdG, ≤], 37 °C [*R*-α-CH_3-γ-OH-PdG, ; *S*-α-CH_3-γ-OH-PdG,], and 50 °C [*R*-α-CH_3-γ-OH-PdG, θ; *S*-α-CH_3-γ-OH-PdG, σ].

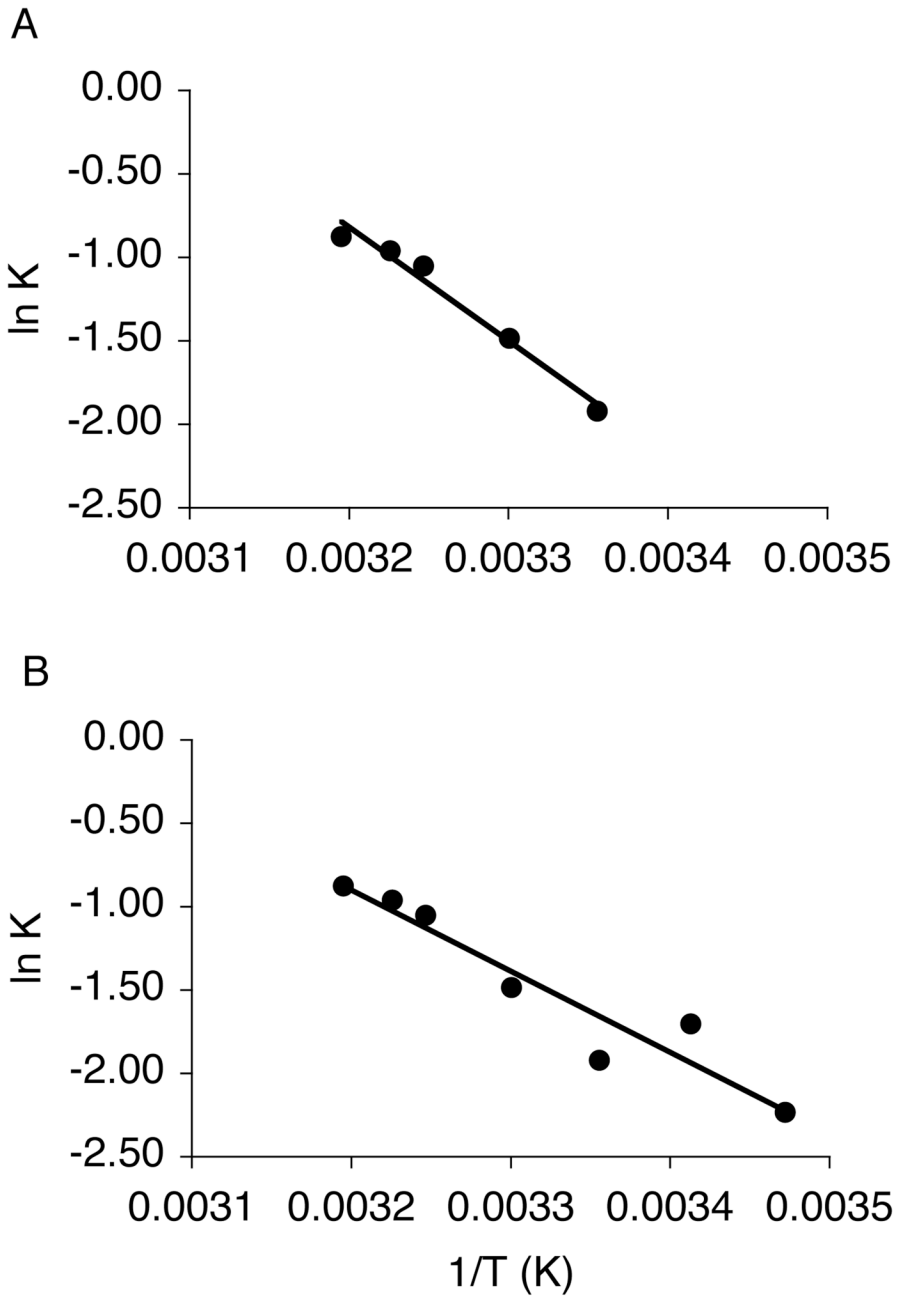

Figure 3.

van't Hoff analysis of the epimerization of *R*- and *S*-α-CH_3-γ-OH-PdG adducts **2a** and **2b** in the oligodeoxynucleotide 5′-d(GCTAGCXAGTCC)-3′. **A.** *R*-α-CH_3-γ-OH-PdG, adduct **2a.** $\Delta H_{cis \rightarrow trans}$ = −14 kcal/mol; $\Delta S_{cis \rightarrow trans}$ = −42 cal/mol K. **B.** *S*-α-CH_3-γ-OH-PdG, adduct **2b.** $\Delta H_{cis \rightarrow trans}$ = −10 kcal/mol; $\Delta S_{cis \rightarrow trans}$ = −29 cal/mol K.

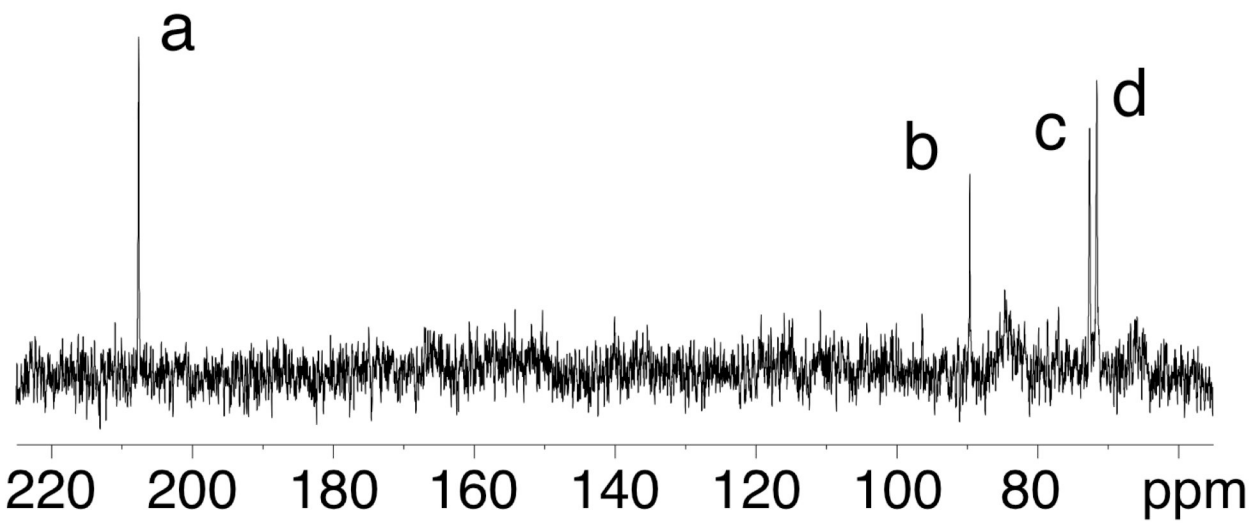

Figure 4.
^{13}C NMR spectrum of *R*-α-CH_3-γ-OH-PdG in the oligodeoxynucleotide 5′-d (GCTAGCXAGTCC)-3′•5′-d(GGACTCYCTAGC)-3′. Resonances a, aldehyde **3a**; b, hydrated aldehyde **4a**; c, carbinolamine crosslink **5a**; d, cyclic adduct **2a**.

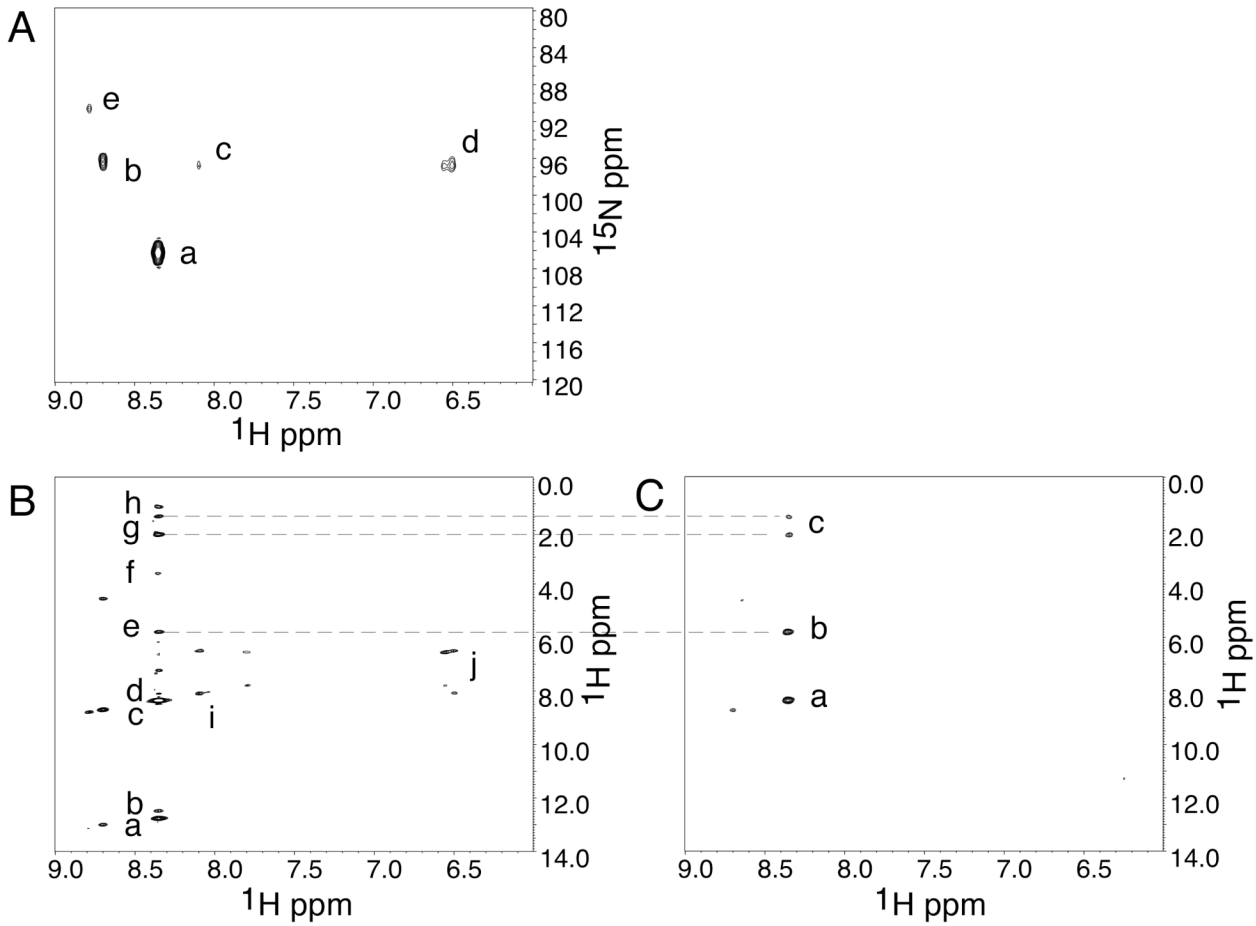

Figure 5.

A. ^{15}N HSQC spectrum of *R*-α-CH_3-γ-OH-PdG in the oligodeoxynucleotide 5′-d (GCTAGCXAGTCC)-3′•5′-d(GGACTCYCTAGC)-3′. Crosspeaks a, major stereoisomer of the carbinolamine crosslink **5a**; b, minor stereoisomer of the carbinolamine crosslink **5a**; c, d, hydrogen- and non-hydrogen-bonded $^{15}N^{2}$H protons of non-crosslinked base pair C^{6}•Y^{19}; e, unidentified crosspeak. **B.** ^{15}N NOESY HSQC spectrum. Crosspeaks a, Y^{19} $^{15}N^{2}$H→Y^{19} N1H; b, Y^{19} $^{15}N^{2}$H→X^{7} N1H; c,Y^{19} $^{15}N^{2}$H autocorrelation; d, Y^{19} $^{15}N^{2}$H→X^{7} N^{2}H; e, Y^{19} $^{15}N^{2}$H→H_{γ}; f, Y^{19} $^{15}N^{2}$H→H_{α}; g, Y^{19} $^{15}N^{2}$H→$H_{\beta'\beta''}$; h, Y^{19} $^{15}N^{2}$H→α-CH_3; i, j, hydrogen-and non-hydrogen-bonded $^{15}N^{2}$H protons of non-crosslinked pair C^{6}•Y^{19}. **C.** ^{15}N TOCSY HSQC spectrum. Crosspeaks a, autocorrelation peak for major stereoisomer of carbinolamine crosslink **5a**; b, coupling to H_{γ}; c, couplings to $H_{\beta',\beta''}$.

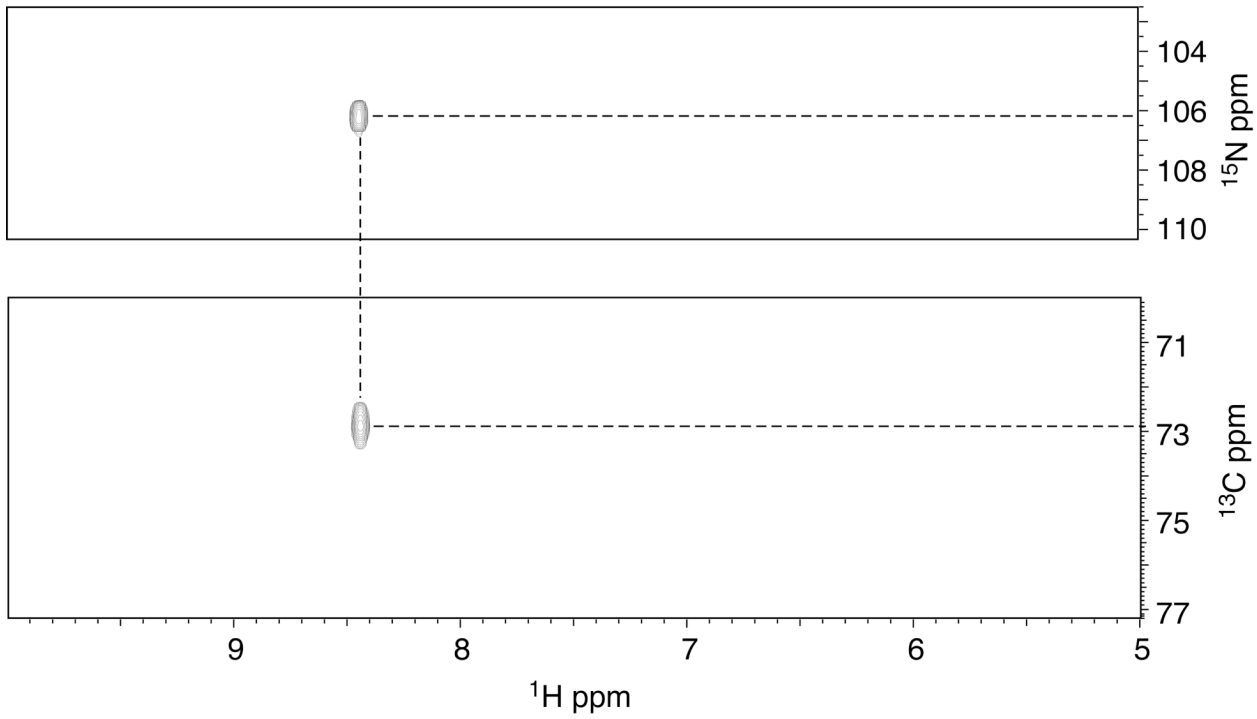

Figure 6.

Triple resonance $^{1}H^{15}N^{13}C$ spectrum of *R*-α-CH_3-γ-OH-PdG in the oligodeoxynucleotide 5′-d(GCTAGCXAGTCC)-3′•5′-d(GGACTCYCTAGC)-3′, confirming the presence of crosslinked carbinolamine **5a**.

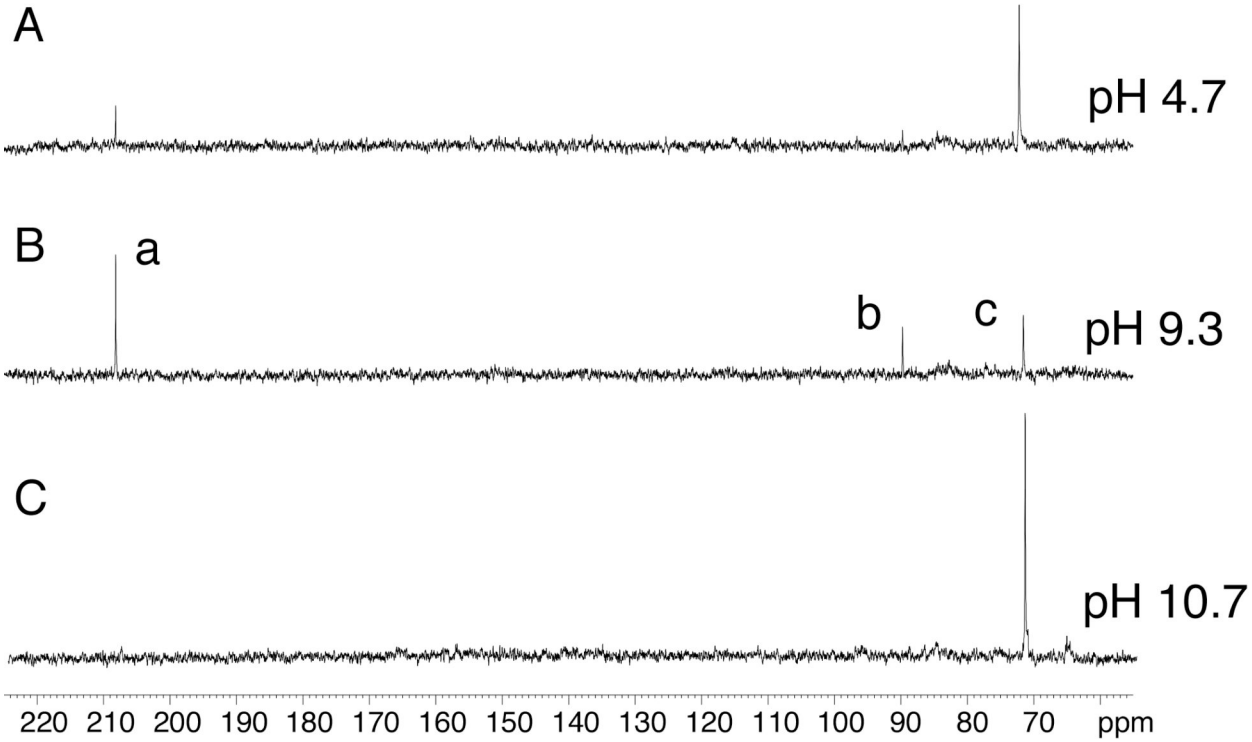

Figure 7.

Chemical species arising from *S*-α-CH_3-γ-OH-PdG in the oligodeoxynucleotide 5′-d(GCTAGCXAGTCC)-3′•5′-d(GGACTCYCTAGC)-3′ as a function of pH. A. pH 9.3. B. pH 10.7. C. pH 4.7. Crosspeaks a, aldehyde **3b**; b, hydrated aldehyde **4b**; c, cyclic adduct **2b**.

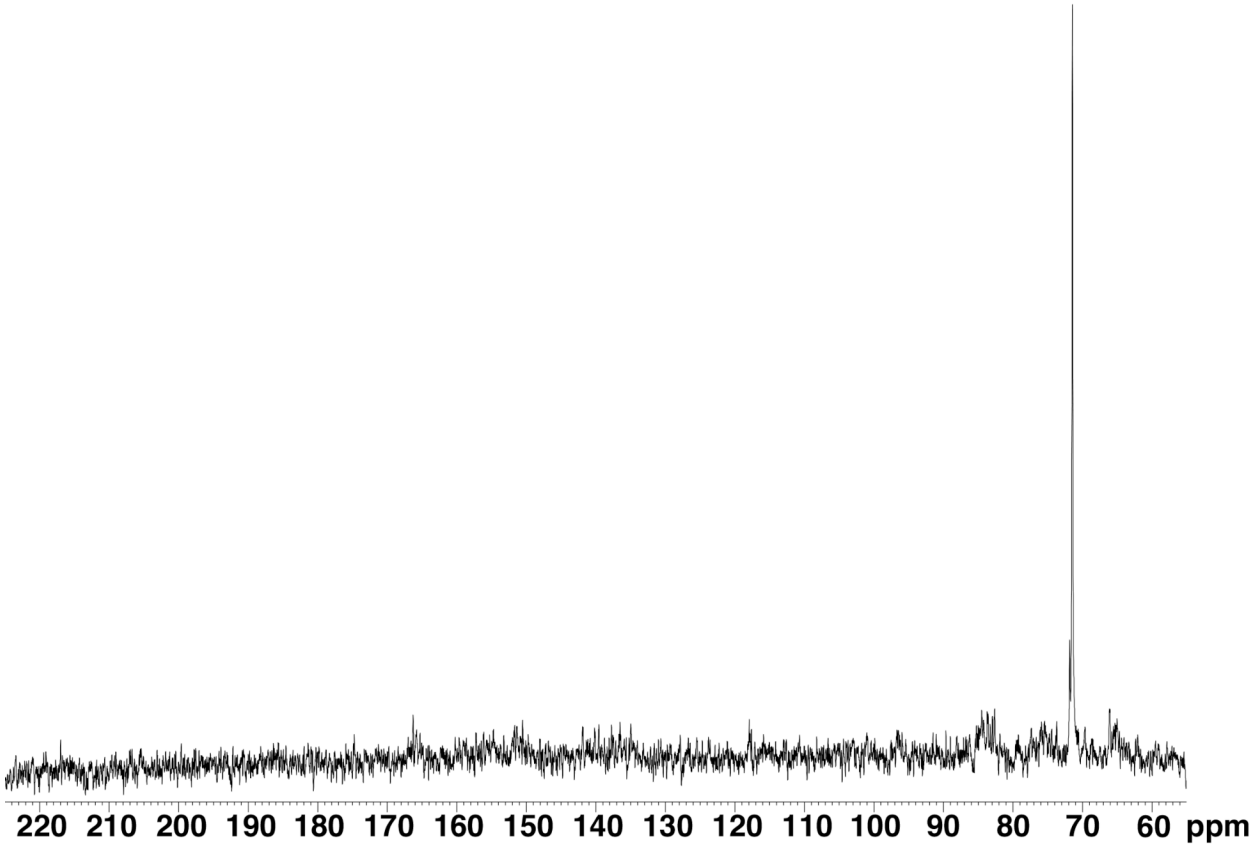

Figure 8.
^{13}C NMR of *S*-α-CH_3-γ-OH-PdG in the oligodeoxynucleotide 5′-d(GCTAGCXAGTCC)-3′ •5′-d(GGACTTGCTAGC)-3′. Only cyclic adduct **2b** is observed.

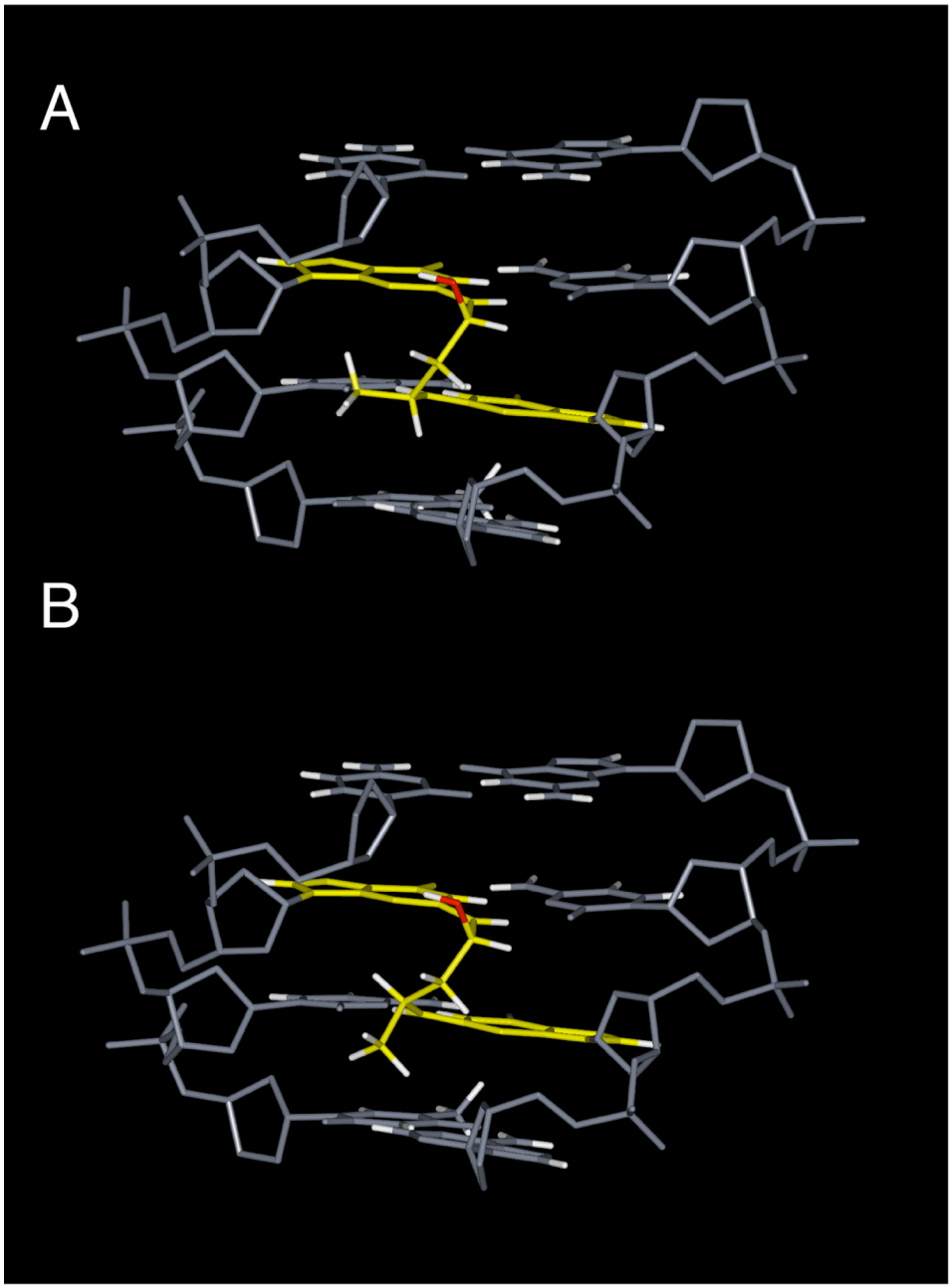

Figure 9.
Molecular modeling of carbinolamine interstrand crosslinks formed in the 5′-CpG-3′ sequence by the *R*- and *S*-α-CH_3-γ-OH-PdG adducts **2a** and **2b**. **A.** Crosslink formed by *R* adduct **2a**. **B.** Crosslink formed by *S* adduct **2b**.

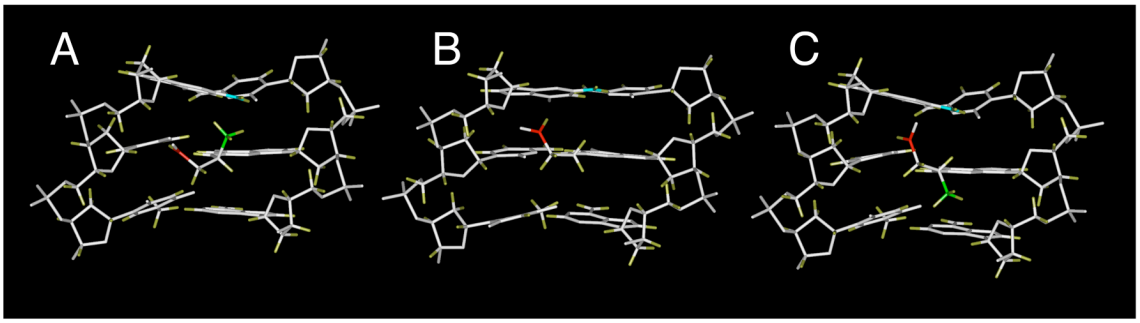

Figure 10.

Molecular modeling of aldehydes **3a** and **3b** formed in duplex DNA when adducts **2a** and **2b** are placed opposite dC in the complementary strand. **A.** Adduct **3b** arising from *S*-α-CH_3-γ-OH-PdG adduct **2b**, illustrating the 5′-minor groove orientation of the α -carbon methyl group. **B.** The N^2-(3-oxo-propyl)-dG aldehyde formed by the acrolein-derived γ-OH-PdG adduct in duplex DNA. **C.** Adduct **3a** arising from *R*-α-CH_3-γ-OH-PdG adduct **2a**, illustrating the 3′-minor groove orientation of the α-carbon methyl group.

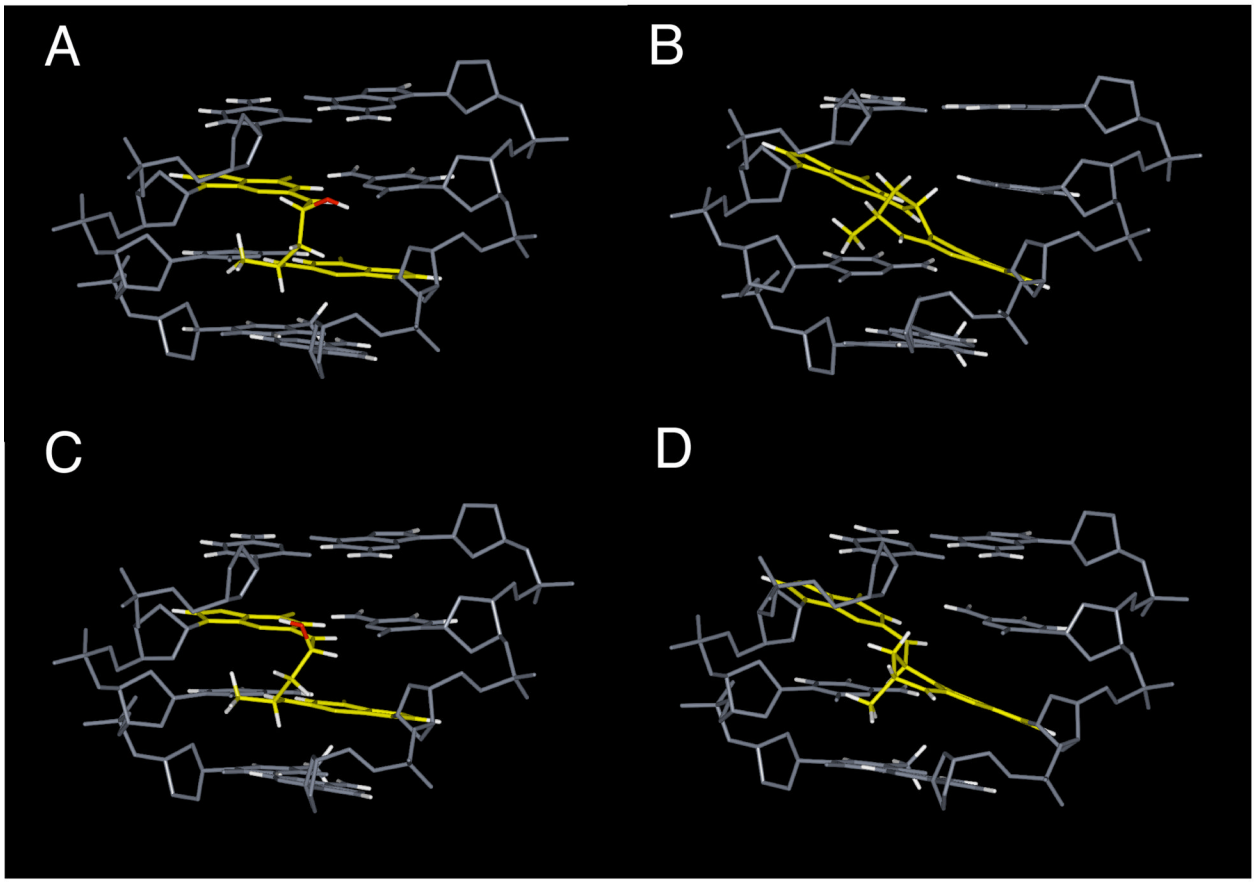

Figure 11.
Molecular modeling of diastereomeric carbinolamine and pyrimidopurinone crosslinks formed by aldehyde **3a**, arising from *R*-α-CH_3-γ-OH-PdG adduct **2a**. **A.** The *R*-diastereomer at the α-carbon of the carbinolamine crosslink. **B.** The *R*-diastereomer at the α-carbon of the pyrimidopurinone crosslink. **C.** The *S*-diasteromer at the α-carbon of the carbinolamine crosslink. **D.** The *S*-diastereomer at the α-carbon of the pyrimidopurinone crosslink.

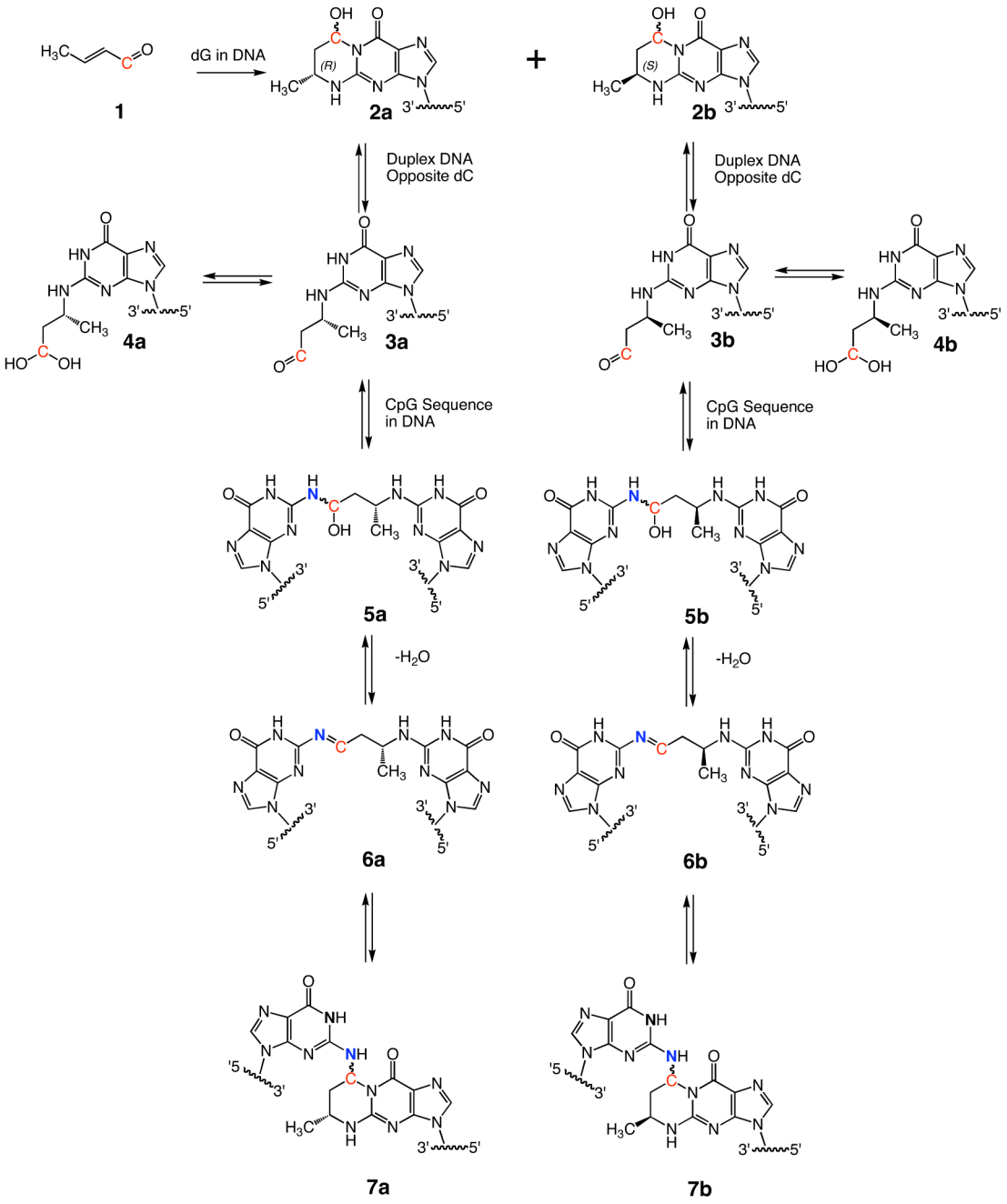

Scheme 1.

Equilibrium Chemistry of the *R*- and *S*-α-CH_3-γ-OH-PdG Adducts in the 5′-CpG-3′ Sequence in Duplex DNA.

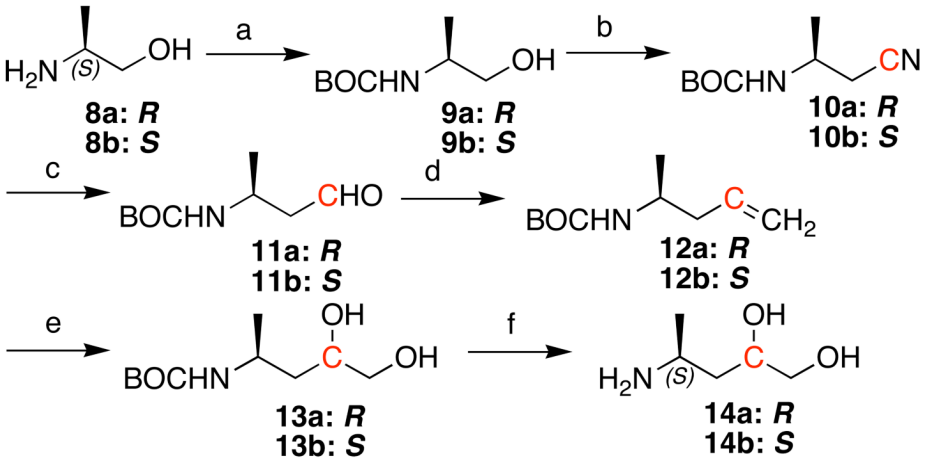

Scheme 2.

Preparation the ^{13}C-labeled amino diols used for site-specific synthesis of adducts **2a** and **2b** in oligodeoxynucleotides. The *S* diastereomer is shown. Reagents: (a) $(Boc)_2O$, 1 M NaOH, overnight, 81.5%, (b) MsCl, Et_3N, CH_2Cl_2, rt, 2 hr; $K^{13}CN$, DMSO, 40 °C, 15 hr, 69% over 2 steps, (c) DIBAH, CH_2Cl_2, −78 °C, 32%, (d) Me_3PCH_2Cl,t-BuOK, THF, 70%, (e) OsO_4, NMP, THF/t-BuOH/H_2O, 76%, (f) Amberlist-H, CH_2Cl_2/CH_3OH; 4 M NH_3 in CH_3OH, 91%. The antipodal 4*R*-enantiomer **14a** was prepared by an identical sequence starting from commercially available (*R*)-2-amino-1-propanol.

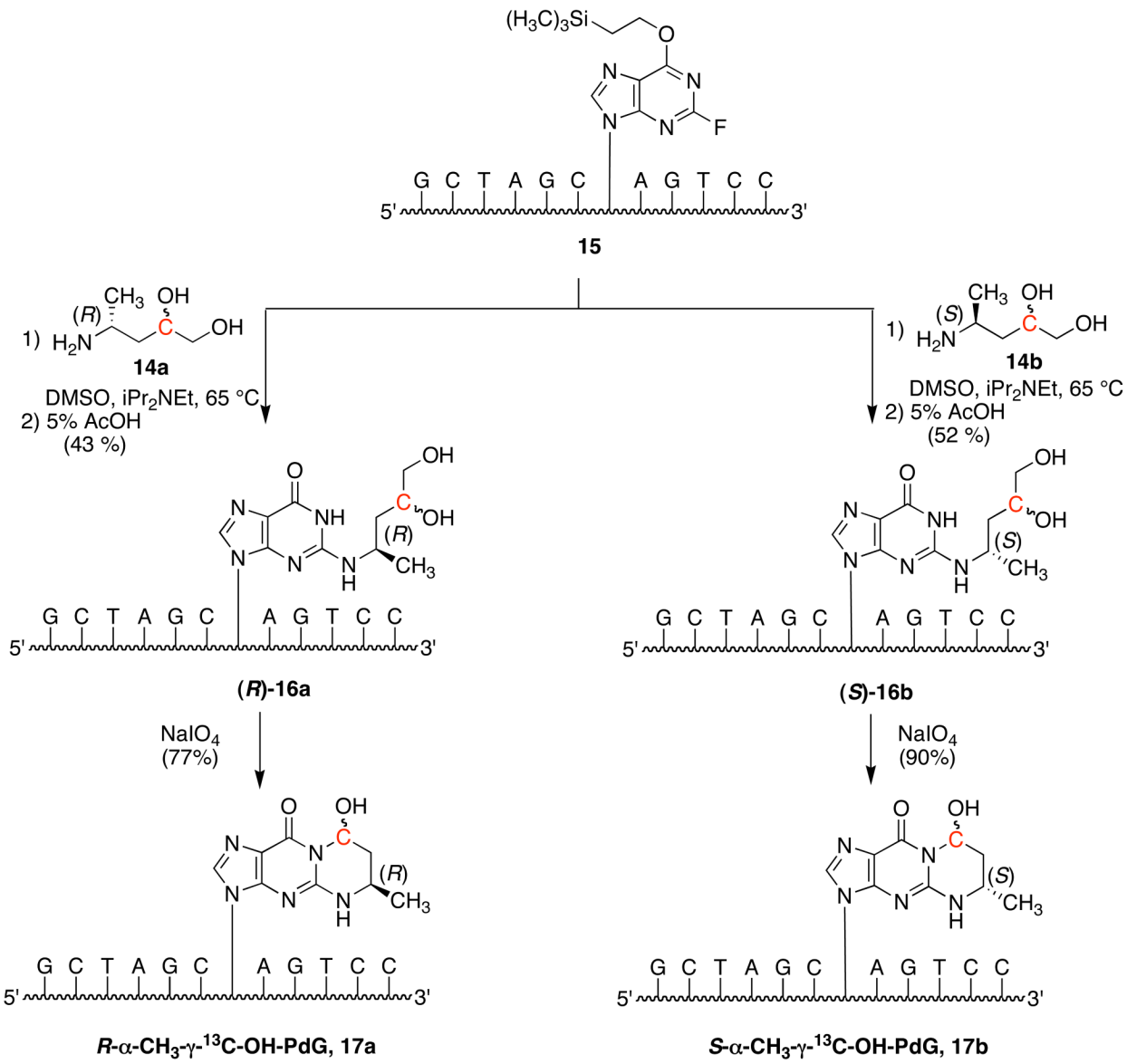

Scheme 3.

Site-specific synthesis of the ^{13}C-labeled oligodeoxynucleotides **17**, **17a** containing adducts **2a** and **2b**.

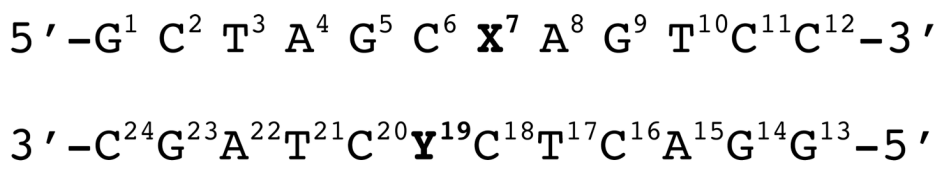

Scheme 4.
The duplex oligodeoxynucleotide containing the 5′-CpG-3′ sequence context. X = α-CH_3-γ-^{13}C-OH-PdG; Y = $^{15}N^2$-dG.